GROWTH OF InGaN MATERIAL AND DEVICE STRUCTURES IN A HIGH PRESSURE MOCVD REACTOR

by

Matthew David Conway

A thesis submitted to the faculty of
The University of North Carolina at Charlotte
in partial fulfillment of the requirements
for the degree of Master of Science in
Electrical Engineering

Charlotte

2019

Approved by:

_____
Dr. Edward Stokes

_____
Dr. Abasifreke Ebong

_____
Dr. Yogendra Kakad

ABSTRACT

MATTHEW DAVID CONWAY. Growth of InGaN material and device structures in a high pressure MOCVD reactor (Under the direction of DR. EDWARD BRITTAIN STOKES)

This is an initial investigation of the super-atmospheric (1.5 – 2.5 bar(a)) Metal-Organic Chemical Vapor Deposition (MOCVD) growth of InGaN materials and experimental, device-like structures. The work was accomplished in a custom MOCVD reactor, specifically designed to produce laminar flow, at super-atmospheric pressures. Four main thrusts are included in this work; initial investigations into total group III flux and V:III ratio, barrier layer growth, and the effect of two growth conditions on photoluminescence, growth temperature and growth pressure/NH_3 partial pressure. Practical limits on the Group-III flux were established. It was discovered that the group-III flux was a very important criteria, in the growth process. A rate that was too high, would cause group-III metals, especially indium, to be deposited on the surface of the substrate, but not incorporated into the crystal lattice.

It was found that higher temperatures were required to produce photoluminescent materials in this high-pressure reactor, than in comparable low-pressure growths. The reasons for this are not well understood.

The samples were all grown on sapphire substrates with a previously grown HVPE GaN layer on top. Preliminary work was performed on the buffer/nucleation layer. The current buffer/nucleation layer is still not completely epitaxial, and this is thought to be a major limiting factor on the current quality of the material and device-like structures in this work. However, this work significantly improved the buffer/nucleation layer, from its

initial state, and has identified several important factors for improving the quality of the buffer layer and ultimately, opto-electronic devices.

Also, photoluminescence over growth pressure and NH_3 partial pressure was investigated. The samples in this thrust were grown from 1.5 bar(a) to 2.5 bar(a) or 0.55 to 0.91 bar(a) NH_3 partial pressure. The results indicate that the photoluminescent efficiency of the samples increased, as their growth pressure increased.

This work concludes with a preliminary recipe for photoluminescent InGaN, at super-atmospheric pressures and initial data, relating photoluminescence to specific process variables. The current growth recipe is given at the conclusion of this work. This recipe is not yet commercial quality; its photoluminescent intensity is not high enough (low IQE), and the growth mode, in the produced samples, is not epitaxial enough. The two issues are thought to be highly related.

ACKNOWLEDGEMENTS

The author would like to thank God, my wife, my family and church for continuous support during the process of this work. I would like to thank Professor Edward Stokes for taking me on as an undergraduate and trusting me with the responsibility of this work, which was a great opportunity and learning experience. I would like to thank my committee, Dr.Aba Ebong and Dr.Yogendra Kakad, who have always been incredibly fair with me, supported me, and been available for professional and academic advice.

Furthermore, I would like to acknowledge the National Science Foundation for their support through two grants:

- #0821590 “MRI: Development of a high-pressure MOCVD for III-nitride semiconductor devices”,
- 1343541 “I-Corps: Improvements in III-Nitride Materials and Devices through Superatmospheric Epitaxy”

and the UNC Charlotte Energy Production and Infrastructure Center (EPIC) for related Graduate Research Assistantships and Travel grants.

TABLE OF CONTENTS

LIST OF TABLES ix

LIST OF FIGURES x

LIST OF SYMBOLS/ABBREVIATIONS xii

CHAPTER 1: INTRODUCTION 1

CHAPTER 2: MOCVD ADDITIONS, MODIFICATIONS, AND DEVELOPMENT 20

2.1 Indium Alloy Capabilities 20

2.2 Automatic Recipe and Control Software 23

2.3 Reactor Inlet Gas Separator: Gas Delivery Turbulence Reduction 26

CHAPTER 3: EXPERIMENTAL METHODS 28

3.1 InGaN Thin Film Studies 28

3.1.1 Group-III Flux Investigation 29

3.1.1.1 Follow Up Experiment: Lower In:Ga Ratio, Higher Temperature 30

3.1.2 Photoluminescence and Growth Temperature Investigation 31

3.2 Multiple Quantum Well Studies 32

3.2.1 Buffer Layer Investigation 32

3.2.1.1 Initial Buffer Layer Growths 32

3.2.1.2 Buffer layer DOE 33

3.2.2 Photoluminescence over Pressure 34

CHAPTER 4: RESULTS AND DISCUSSION 37

4.1 InGaN Thin Film Studies 37

4.1.1 Group-III Flux Investigation Results 37

4.1.1.1 Follow Up Experiment: Lower In:Ga Ratio, Higher Temperature Results 46

4.1.2 Photoluminescence and Growth Temperature Investigation Results 50

4.2 Multiple Quantum Well Studies 53

4.2.1 Buffer Layer Investigation 53

4.2.1.1 Initial Buffer Layer Growths Results 53

4.2.1.2 Buffer layer DOE Results 58

4.2.2 Photoluminescence over Pressure Results 61

CHAPTER 5: CONCLUSIONS 73

5.1 InGaN Thin Film Studies 73

5.1.1 Group-III Flux Investigation Conclusions 73

5.1.1.1 Follow Up Experiment: Lower In:Ga Ratio, Higher Temperature Conclusions 74

5.1.2 Photoluminescence and Growth Temperature Conclusions 74

5.2 Multiple Quantum Well Studies 74

5.2.1 Buffer Layer Investigation 74

5.2.1.1 Initial Buffer Layer Growths Conclusions 74

5.2.1.2 Buffer Layer DOE Conclusions 75

5.2.2 Photoluminescence over Pressure Conclusions 75

CHAPTER 6: RECOMMENDATIONS 77

REFERENCES 79

APPENDIX A: HIGH PRESSURE MOCVD STANDARD OPERATING PROCEDURES 85

APPENDIX B: RECIPE FOR InGaN MATERIAL AND MQW GROWTH IN HIGH PRESSURE MOCVD 89

APPENDIX C: SAMPLE GROWTH PARAMETERS AND STRUCTURES 90

LIST OF TABLES

TABLE 1: Sample numbers and buffer layer parameters 33

TABLE 2: Buffer layer temperature and thickness DOE 34

TABLE 3: Pressure experiment samples and respective changed parameters 36

TABLE 4: X-Ray fluorescence data of HP11, revealing excess indium deposition 44

TABLE 5: X-Ray fluorescence data of HP16, showing improvement in composition 45

TABLE 6: Minimum, maximum, and average group-III content. HP16 does not include objects. 46

TABLE 7: HP23's X-Ray fluorescence results, showing data similar to industry grown templates 47

TABLE 8: Corresponding buffer layer and binary PL data 54

TABLE 9: Pressure experiment samples and respective changed parameters 63

TABLE 10: Thermocouple and fitted temperatures at various pressures 65

TABLE 11: Samples with corrected temperature data 66

TABLE 12: Photoluminescence data for samples HP76, HP78, and HP79 66

TABLE 13: 78ºK IQE estimate 66

LIST OF FIGURES

FIGURE 1: Bandgaps and *a* lattice constants of the III-Nitrides 2

FIGURE 2: Hexagonal Wurtzite and unit cell for III-Nitrides 3

FIGURE 3: 2018 external quantum efficiencies of emitters (T_J = 25ºC, J = ~350mA/mm^2) and the human eye response, adapted from data in [1] 5

FIGURE 4: III-Nitride MOCVD precursors going through pyrolysis and reactions to form epitaxial crystal layers 9

FIGURE 5: Gas inlet to CFD-design high pressure reactor, showing separated NH_3 and MO regions, with an N_2 curtain 10

FIGURE 6: Nominal diagram of UNCC's CFD-designed high pressure reactor 14

FIGURE 7: Three iterations of reaction chamber CFD design. The turbulence is pushed further into the exhaust with each iteration. 16

FIGURE 8: Quantum efficiency vs VH_3 partial pressure for different V-III semiconductor families, as well as the possibility of a III-Nitride curve 18

FIGURE 9: Original design for the HP-MOCVD gas delivery system 21

FIGURE 10: Diagram of MO bubbler and gas lines 22

FIGURE 11: Main tab of the HP-MOCVD control software 24

FIGURE 12: HP-MOCVD Recipe Writer main screen, showing the same layout as the main control program 25

FIGURE 13: HP-MOCVD Recipe Writer bubbler tab 26

FIGURE 14: Gas separator insert, later refabricated to match flows and keep design consistent with simulation(s) 27

FIGURE 15: MQW structure for IQE vs pressure experiments 35

FIGURE 16: SEM image showing a pumice-like surface on HP11 38

FIGURE 17: SEM image, showing a smoother surface on HP16, grown with HP17 recipe 39

FIGURE 18: X-Ray diffraction of HP11, HP13, and HP17, showing decreasing In peaks 40

FIGURE 19: Indium metal peak XRD intensities for HP11, HP13, and HP17 41

FIGURE 20: HP23's 78.5°K and 295°K PL spectrums, showing a small InGaN peak. Inset: close up of InGaN peak 48

FIGURE 21: 2θ-ω XRD scan of HP23, showing InGaN diffraction peaks 49

FIGURE 22: PL of HP38, HP39, and HP40, showing increased intensity with growth temperature 51

FIGURE 23: Graph, showing increase in 78K PL intensity with growth temperature 52

FIGURE 24: XRD plot of HP40 confirmed crystalline InGaN growth 53

FIGURE 25: AFM of HP54, grown with no buffer layer, showing island growth 55

FIGURE 26: AFM of HP57, grown with a high temperature buffer layer, showing islands coalescing 55

FIGURE 27: Illustration of nucleated islands, coalescing during growth 57

FIGURE 28: High temperature buffer layer DOE results showing PL intensity relative to the 5nm, 1100ºC sample, which was normalized to 1 60

FIGURE 29: Luminescent intensity vs growth pressure/NH_3 partial pressure 67

FIGURE 30: InGaN emission peak, blue shifting with increased pressure 69

FIGURE 31: FWHM and FWHM Δ vs pressure 70

FIGURE 32: IQE figure of merit vs pressure 71

LIST OF SYMBOLS/ABBREVIATIONS

DOE	Design of experiments
EDAX	X-Ray fluorescence instrument, with multiple additional detectors
IQE	internal quantum efficiency
IQE FOM	internal quantum efficiency figure of merit
MOCVD	metal organic chemical vapor deposition
MQW	multiple quantum well
PL	photoluminescence
SEM	scanning electron microscope/microscopy
SQW	single quantum well
XRD	X-Ray diffraction

CHAPTER 1: INTRODUCTION

This work is an investigation into epitaxial growth of gallium nitride (GaN) and indium gallium nitride (InGaN) materials and device structures at super-atmospheric pressures. The focus is on understanding and developing growth processes, with the intent of progressing this area of research towards the production of high-quality optoelectronics across a wide range of bandgaps. Epitaxial growth was done in a Metal-Organic Chemical Vapor Deposition (MOCVD) reactor, which was designed using computation fluid dynamics (CFD). The super-atmospheric MOCVD reactor was design and constructed through a Major Research Instrumentation grant, from the National Science Foundation [2].

The interest in the III-N, which are III-V semiconductors, with the group V element being nitrogen, is largely based upon their potential for a wide range of optoelectronic applications. III-N alloys have bandgaps that range from indium nitride (InN) around 0.7eV to aluminum nitride (AlN) at 6.2eV, with gallium nitride (GaN) in between, at 3.4eV, which can be seen in Figure 1 [3] [4].

These bandgaps correspond to wavelengths from 1771nm to 200nm, encompassing the main IR wavelengths for optical communications, 1530-1560nm, the entire visible spectrum, and UV wavelengths that are useful for disinfecting, curing, and sensing.

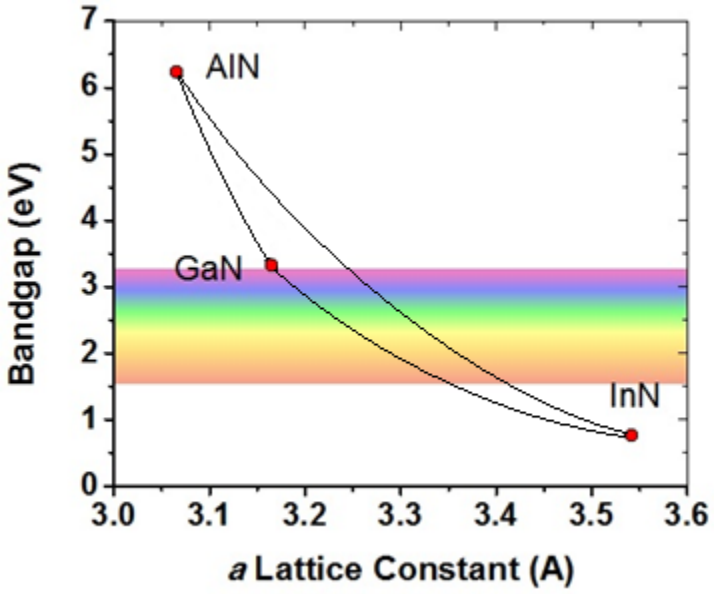

Figure 1: Bandgaps and *a* lattice constants of the III-Nitrides

The III-Nitrides that are investigated in this work form lattices with hexagonal, wurtzite cell structures, as seen in Figure 2. The III-Nitrides are normally grown along the *c* axis, and would ideally be grown on a native, or lattice-matched substrate to achieve optimum quality [3]. Inconveniently, bulk GaN, the ideal substrate, is still a heavily researched topic, with few commercial options available [5]. This means GaN and InGaN must be grown on the next suitable material, which is traditionally sapphire (Al_2O_3). SiC has recently increased in popularity, because it has a better lattice match. Companies, such as CREE, have shown its value in production, but it is relatively expensive compared to sapphire.

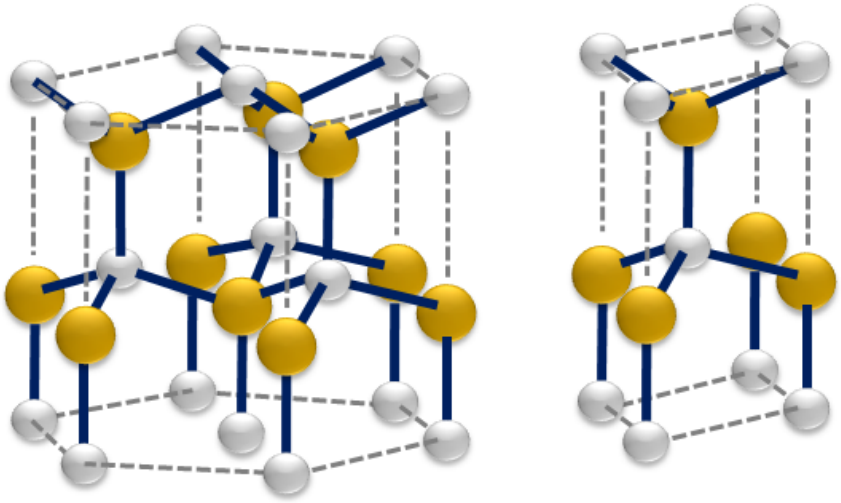

Figure 2: Hexagonal Wurtzite and unit cell for III-Nitrides

Already a major player in light emitting diodes for solid state lighting, once academic and industrial research has produced mature manufacturing processes for the entire composition range, the III-Nitrides have the potential to move into other areas, such as ultraviolet emitters, solar cells, and near infrared optical communications. Currently, there is a wide range of materials in optoelectronics, each for different applications. For instance, devices with wavelengths that are amber colored or longer, are currently made with other material groups, namely the III-Arsenides and III-Phosphides. The ability to manufacture high quality, crystalline material across the whole composition range of the III-Nitrides, would eliminate the need for the majority of equipment and inventory that is related to other material systems. This would also allow one manufacturer to easily create many device and work in many areas of opto-electronics without large investments in new capital and having to house multiple MOCVD systems to grow devices in different bandgap and wavelength ranges. Although such a solution may be years in the future, it could produce simplification of manufacturing and achieve cost savings.

In addition to the possible cost savings, complete processing conditions for the full range of III-Nitride material would allow for new, previously inaccessible devices to be made. This is due to the fact that many different band gaps could be grown, in the same reactor, allowing devices with different compositional layers to be grown. The ability to grow layers with band gaps across such a wide range could allow multi-colored and tunable spectrum devices to appear on the horizon, as emitters, detectors, or energy harvesting devices.

This work is primarily on the ternary III-Nitride alloy, InGaN, which has the potential to make devices with wavelengths ranging from 1771nm (InN) to 365nm (GaN), which is the entire visible spectrum, the near-IR, and the approximate wavelengths of 400nm -365nm in the UV spectrum. InGaN is currently the primary material used for blue LEDs, blue lasers, and white LEDs that employ phosphor down-conversion to obtain longer wavelength, broader spread spectrums that we perceive as white. The standard, white LED bulbs for household use, generally employ such techniques due to the difficulty of growing optical quality InGaN material with indium contents greater than 20 -25% [6] [7]. This severely constrains the potential of InGaN; limiting the useable wavelengths to blue, near-UV, and some blue-greens.

This difficulty, along with the current availability of bandgap energies in other materials, has led to what is known as the “Green Gap”. As the indium content in InGaN LEDs is increased, and therefore the wavelength, the ability of the current manufacturing processes to produce LEDs with high internal quantum efficiency (IQE) degrades [7]. This is due to limitation in current manufacturing processes, lack of lattice-matched substrates, and the physical and thermodynamic properties of the materials themselves [8]. The green

gap is an even more desirable problem to solve, as the green gap overlaps the peak human eye response, meaning efficient emitters in this range of the visible spectrum would allow significant energy saving, if put into mass use. The overlap and 2018 data can be seen in Figure 3.

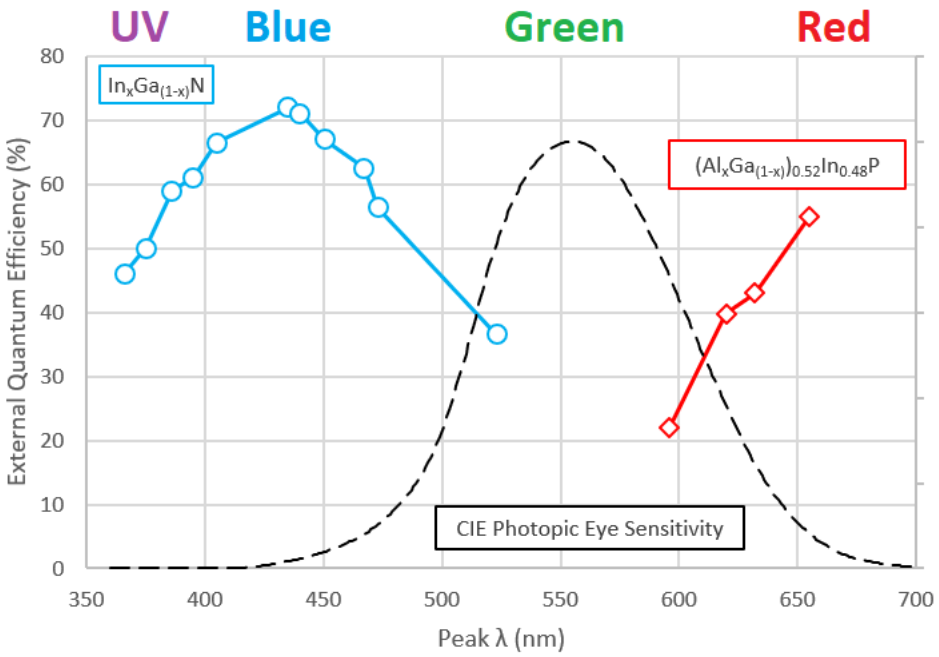

Figure 3: 2018 external quantum efficiencies of emitters (T_J = 25ºC, J = ~350mA/mm^2) and the human eye response, adapted from data in [1]

One factor is the size difference between the indium and gallium atoms. This difference alone has led some to speculate on the possibility of manufacturing compositions such as 50% indium and 50% gallium, as well as the possibility of early degradation of material with such compositions, due to internal material stresses. This is also related to the different lattice constants in the binary materials, with the *a* lattice constant for InN being around 3.54Å and GaN being around 3.19Å [9]. This makes large compositional differences in heterostructures difficult, as strain is introduced, making high

quality, high indium content material especially difficult to grow [10]. It is also due to the fact that a suitable, lattice-matched substrate has not been found for the larger lattice constants of InN and InGaN alloys. Because Al_2O_3 and SiC are the primary substrates, both having lattice constants smaller than GaN, thick GaN is usually grown first. This is done to obtain a minimum of relaxed GaN material before larger lattice constant material, such as InGaN film or wells, is grown.

Commercially, III-Nitride materials are most commonly synthesized by metal-organic chemical vapor deposition (MOCVD). MOCVD is proven to have significantly faster growth rates and to be better suited to multi-wafer fabrication than methods like molecular beam epitaxy (MBE). In an MOCVD system, there is also significant flexibility to change growth rates and grow very thin, high quality layers, as well as bulk material. This enables active layers, on the order of single nanometers, to be grown on top of bulk GaN, on the order of several μm.

On a high level, an MOCVD system is generally comprised of chemical precursors, a gas delivery system, and a reaction chamber, along with the necessary vacuum pump(s), exhaust filter(s), and control system(s). The substrate is held in the reaction chamber, which usually contains a substrate heater, exhaust ports, gas inlets and in-situ monitoring. The epitaxial material is grown in the reaction chamber, through a chemical reaction consisting of pyrolysis of the precursor gasses and the subsequent reactions that ideally produce solid phase optical semiconductors. However, there are estimated to be at least 60 reaction pathways that can occur and some of them are not favorable to the production of high-quality crystals. A significant number of different chemicals can be used as precursors for the synthesis reaction although there are only a few in common usage due to currently

available purity and properties. Ammonia (NH_3) is the most commonly used precursor for the nitrogen component, although it is the precursor with the most interest in finding an alternative. Ammonia has the benefit of being inexpensive and relatively safe, especially compared to arsine, used in the MOCVD of III-Arsenides. However, it has the drawback of low cracking efficiencies below 800°C [11] [12], while InN is normally stable at temperatures below ~550°C [13]. This makes ammonia an inefficient precursor for the growth of III-Nitrides containing indium, as well as any low temperature growth process. Although there is work being done with hydrazine and other chemicals for more efficient nitrogen extraction at lower temperatures, ammonia remains the favored group V precursor for the III-Nitrides. In this work ammonia is used as the exclusive N precursor.

The aluminum, gallium, and indium precursors are the chemicals that MOCVD gets its name from, the metal organics. These precursors are typically three ethyl or methyl groups bonded to one of the elements in the "boron group" (historically known as "group III" and now classified as IUPAC group 13) making triethylgallium (TEG), trimethylindium (TMI), and various other combinations of tri ethyl or methyl groups and boron group atoms. These chemicals are now being produced with the purities necessary for high quality crystal growth. Due to their pyrophoric nature, these chemicals must be kept in a sealed container or "bubbler" and stored in the absence of oxygen. The containers are stainless steel, allowing them to be kept in water baths for temperature control, directly affecting the vapor pressure of the chemical and their molar flow rates.

The MOCVD reaction is a thermo chemical one, with several inherent steps. MOCVD is done at relatively high temperatures, with the low temperature MOCVD of III-Nitrides, usually referring to processes done between 500°C and 650°C. High temperature

reactions are usually on the order of 1000°C to 1200°C. Temperatures are kept this high due to the thermo-chemical nature of the binaries themselves. In the first step(s) of the reaction, the precursors pyrolyze, with some of the organic molecules breaking off, leaving volatile molecules and atoms, ideally, to react on the substrate, producing a crystal film. A series of reactions can also occur, producing III-Nitride crystals on the substrate through intermediate steps. There are multiple chemical paths to crystal growth as seen in Figure 4. There are other reaction pathways that can occur as well, resulting in the inclusion of organic molecules in the crystal lattice and related, quality degrading issues. Part of the process development is minimizing these parasitic reactions.

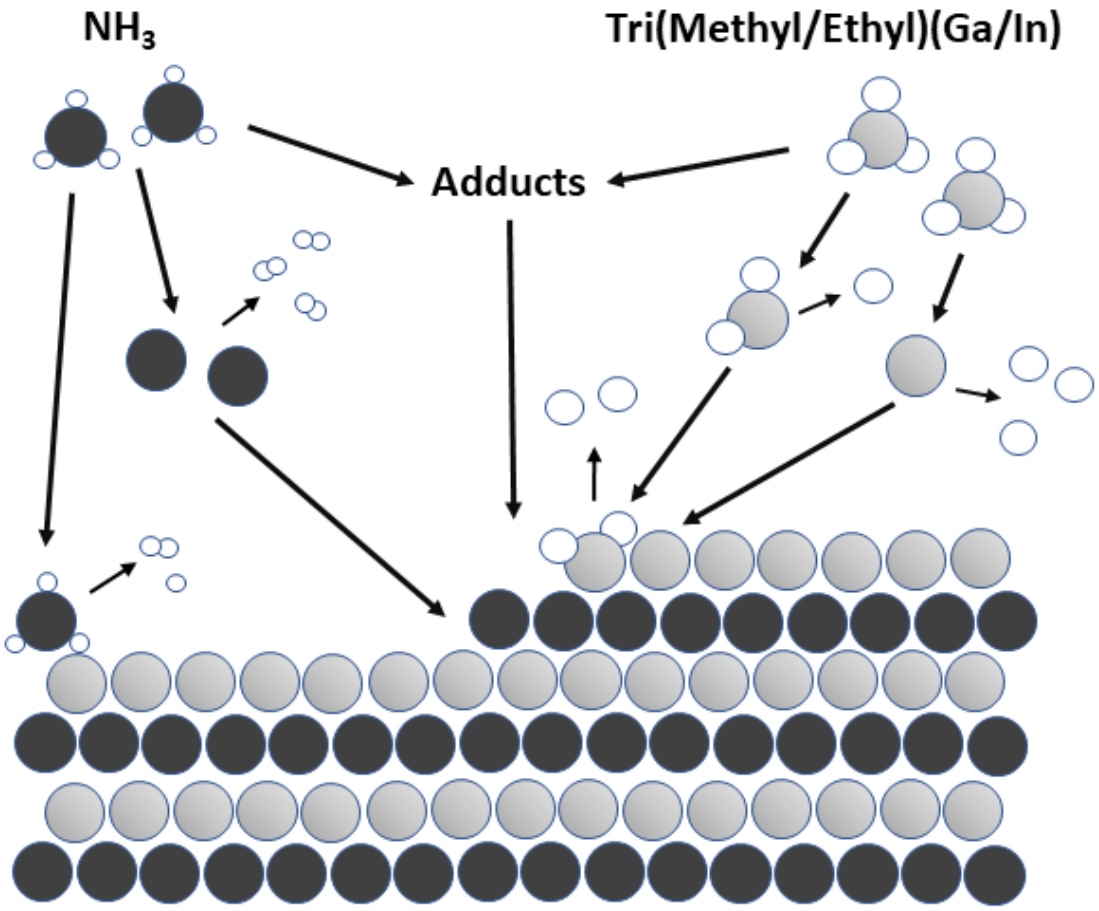

Figure 4: III-Nitride MOCVD precursors going through pyrolysis and reactions to form epitaxial crystal layers

In the CFD-designed high pressure reactor, the gas flow was specifically designed to minimize adduct formation, before the substrate. While standard MOCVD often has mixed or semi-mixed precursors, the high-pressure reactor has the group-III and group-V precursors entering the reactor in different flow regions. There is also a curtain of flowing N_2, between the precursors, to prevent reactions from occurring at the gaseous interfaces, as seen in Figure 5. This is intended to minimize parasitic reactions. Although their work

follows ours [2], Ma et. al. reports success with a spatially separated reactor, although theirs does not include an N_2 curtain at the gas interface [14].

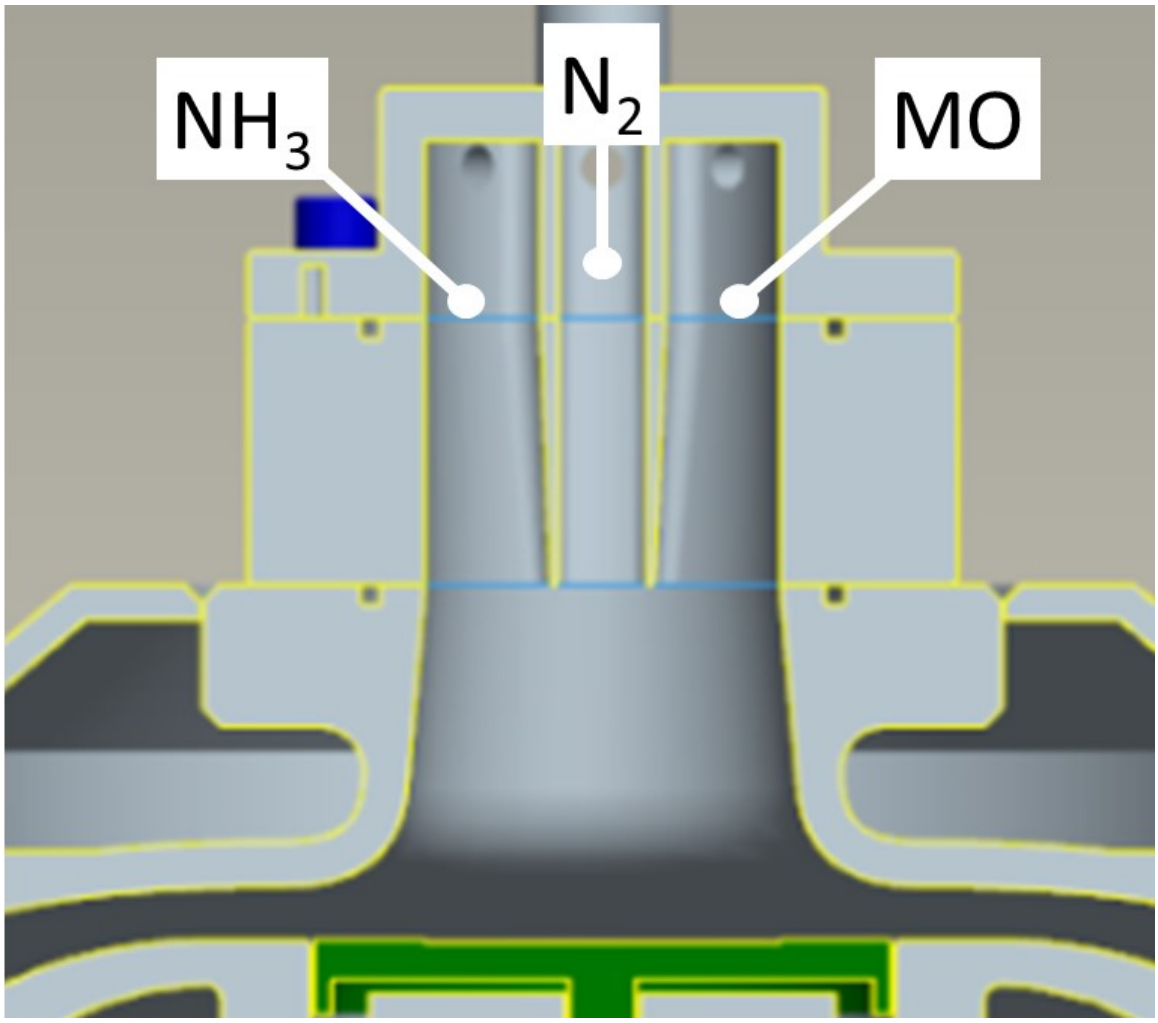

Figure 5: Gas inlet to CFD-design high pressure reactor, showing separated NH_3 and MO regions, with an N_2 curtain

All of the reaction pathways that happen are not completely confirmed, although there has been significant work in the area [12] [15]. The MOCVD process consists of a controlled reaction with the intent to have the product of the reaction be a single, high quality semiconducting crystal film. The high temperature in the high pressure MOCVD,

as seen in Figure 6 is from a heater, directly under the susceptor, with the intent of pyrolyzing the precursor molecules near the substrate. Pyrolyzing near the substrate, assists in the reduction of unfavorable chemical reactions, leaving the desired, volatile elements to react and deposit in an environment that is favorable to crystal growth. The goal of developing processes for the MOCVD system and the intended crystals is to create the most favorable conditions possible for high quality crystal growth.

In the MOCVD of III-Nitrides, specifically, there are several reaction parameters that can have a large effect on the way the precursors react and form crystals. Some of the important metrics are pressure, temperature, V:III ratio, growth rate/total precursor flow, III_1:III_2 ratio, as well as specific reactor geometries that can affect gas flow and temperature gradients on the substrate.

As Figure 1 indicates, the energy gaps of the binary III-Nitride compounds span a significant range. The thermodynamic properties of the binary compounds are also quite different, making the thermodynamic process window narrow and susceptible to slight changes. Although much work has been done to reduce variances on the growth surface, this is the reason even commercial MOCVD systems experience variances in composition and quality over the surface of a single wafer, making binning a necessity.

All three binary compounds decompose at different temperatures and have favorable process conditions that are significantly different from each other.

The InN binary decomposes at significantly lower temperatures than the other binaries, making significant differences in their processing windows. The temperature where InN begins to decompose, or desorb, is around 550°C with conventional low pressure MOCVD [13] [16]. This creates a significant problem, as NH_3 has a very poor

cracking efficiency at temperatures below 800°C and V:III ratios on the order of 10^5 have been reported, in the MOCVD of InN [17]. This is also a problem from the standpoint of crystal growth, as higher temperatures give the III atoms a higher mobility, allowing them to travel to the correct lattice sites. It is well documented that higher temperatures, within certain limits, correspond to higher quality crystal growth, making the low equilibrium temperatures of InN unfavorable to high quality synthesis [18].

Traditional MOCVD is done at low pressures, usually significantly less than half of an atmosphere [18] [19]. This reduces gas phase reactions within the reactor and has the added benefit of keeping the system in an "implosion" state if there were a gas leak, as opposed to the possibility of leaking pyrophoric, metal-organic chemicals into the working environment.

In the current state, synthesis of ternaries, such as InGaN, must compete with such effects as desorption, where the InN is decomposing while the crystal is growing. This is due to the necessary temperatures for growth, which exceed the ~550°C equilibrium line for InN. The growth rate must be faster than the rate of indium desorption to incorporate any indium into the crystal.

Through a conceptual deduction, it can be noted that the greater the desired indium incorporation, the closer the processing conditions must be to stable InN conditions. This is supported by multiple works [20] [21], although lattice mismatch is expected to account for some of the difficulties in growing high indium concentrations. Because conventional MOCVD is done at low pressures and higher temperatures which are somewhat necessary for high quality crystals and effective V atom processing, indium incorporations above 20% have been difficult to achieve [19]. Although samples have been grown with greater

indium incorporations, the quality of the grown crystals decreases with indium composition [10]. This gives rise to the green gap, named for the lack of high efficiency LEDs in the green wavelengths, which correspond to indium incorporations in the range of 26-33%. High efficiency LEDs in the yellow, orange, and red wavelengths have been fabricated with the phosphide material group as indicated in Figure 3.

In the attempt to close the green gap and to find a suitable process window for InGaN with high levels of indium incorporation, high pressure MOCVD is being researched in this work. Some work has been done with atmospheric pressure MOCVD of III-Nitrides [17] [22], as well as increasing the pressure of conventional systems, while staying below one atmosphere [23] [24]. Dietz, et. al. have been studying high pressure MOCVD as well, using a custom, pulsed precursor method [20].

By increasing the growth pressure in the reactor, the decomposition temperature of InN is raised significantly, allowing higher temperature growths, leading to higher quality InGaN [25]. The equilibrium pressure vs temperature line is logarithmic, with an equal increase in decomposition temperature with each decade of atmospheres. This corresponds to over 100°C within the first ten atmospheres.

To investigate the improved processing window at high pressures, a superatmospheric MOCVD reactor was designed at UNCC, with the ECE and ME departments working together, as seen in Figure 6 [2]. At high pressures, the gas flows within the reactors become turbulent, causing gas phase reactions, a significant detriment to quality crystal growth.

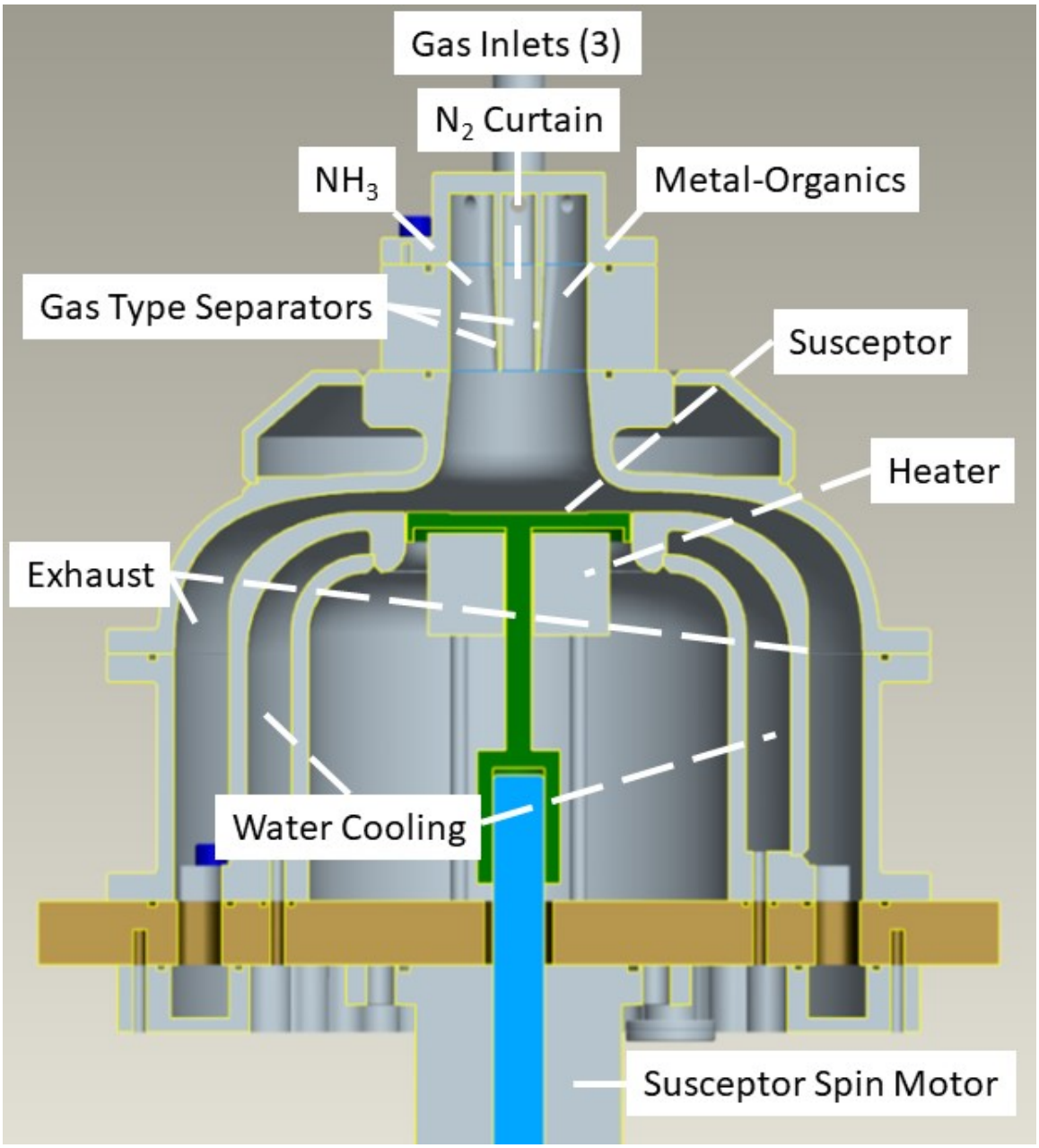

Figure 6: Nominal diagram of UNCC's CFD-designed high pressure reactor

There are several sources of turbulence within a reactor, the Kelvin-Helmholtz, the Rayleigh-Bénard, and the Dean instabilities. The Kelvin-Helmholtz instability is caused by a velocity shear in a single, continuous fluid, or two fluids that have different velocities at their interface. This can happen where the gasses are injected into the reactor, or where the

rotating susceptor interfaces with the incident gasses. The Rayleigh-Bénard instability occurs with temperature gradients. The temperature gradient is also from the susceptor, which is being heated to temperatures from 600°C to 1300°C, with a tungsten element directly below it. This causes convection, and can produce fluid convection cells, if not properly taken care of. The last instability, the Dean instability, can occur if the shape of the reactor is not properly designed for the applicable processing conditions.

The HP-MOCVD system at UNCC was designed with extensive computational fluid dynamics (CFD) to ensure good flow conditions during growth. CFD simulations were done in Star-CCM^{+}, a commercial CFD software package. The reactor was designed from a concept originally put forward by Dr. David Bour [26], which was taken, extrapolated, and put into a quantified, applicable form, displayed above, in Figure 6.

The final design was reached through several iterations of CFD simulations and changes, with the final design reaching acceptable gas flows through the reaction chamber. The near elimination of turbulence in the gas delivery path and susceptor, or growth area, was accomplished by pushing the turbulence into the exhaust channel with the geometry of the reactor. This way any gas mixing and turbulence will happen after the gasses flow over the substrate and should not affect the growth reaction (Figure 7). This work was done in this reaction chamber, with the HP-MOCVD system that accompanies it.

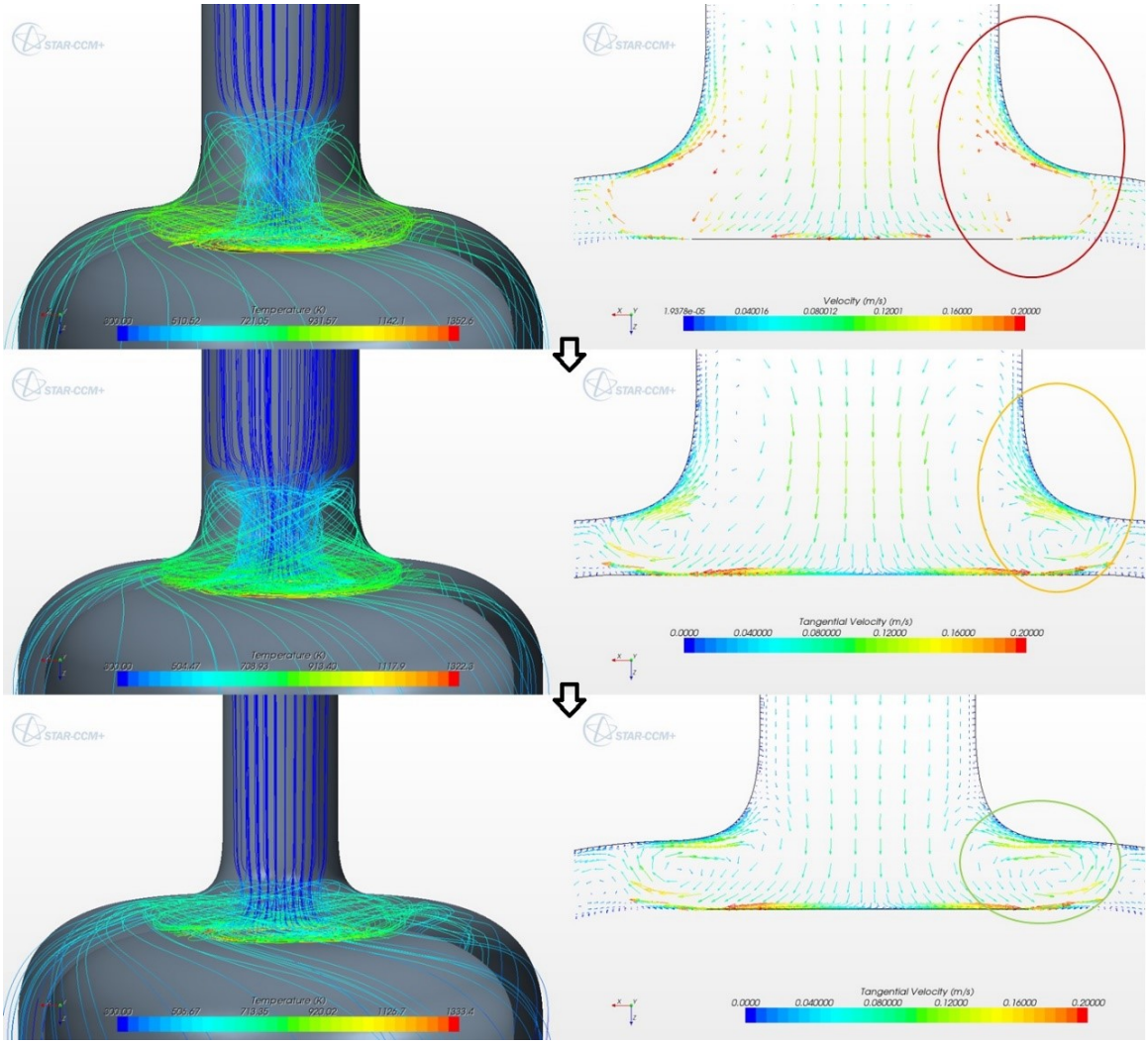

Figure 7: Three iterations of reaction chamber CFD design. The turbulence is pushed further into the exhaust with each iteration.

To understand some of the influential differences in the properties of the binary InN and GaN, the work of MacChesney et. al. is consulted [13]. MacChesney et. al. investigated the thermal stability of InN at high temperatures and pressures in an N_2 ambient. Polycrystalline InN was prepared for the study, following the method given by Juza and Hahn in 1940 [27].

The InN and some indium as a metal, were put into a bomb in an autoclave and equilibrated at pressures between 1 and 1000 atmospheres (bars). The data comprised a logarithmic plot, with a steep rise in dissociation pressure at higher temperatures. The heat of formation was deduced to be 33.4kCal/mol, although it was noted that they did not confirm any observation of InN formation at solid-phase, stable conditions. In this study, the stable P-T relations for stable GaN and AlN phases were graphed and commented on, as well as adding InN to the P-T graph. The data clearly indicates wide phase gaps for GaN and InN, which could be problematic for ternary InGaN synthesis. This indicates that the InN phase decomposes at optimal GaN growth temperatures, although the relation shows that higher pressures would allow InN to be grown at higher temperatures.

Additionally, work in other III-V semiconductors shows a relation between quantum efficiency and group-V hydride partial pressure (VH_3). The III-Arsenides and III-Phosphides, both show this relation and it theorized that the III-Nitrides may as well, as seen in Figure 8. If a quantum efficiency vs VH_3 partial pressure relation exists, the location of the curve has not yet been identified. This reactor allows the increased pressure that may be necessary to find the quantum efficiency vs VH_3 partial pressure relation for the III-Nitrides.

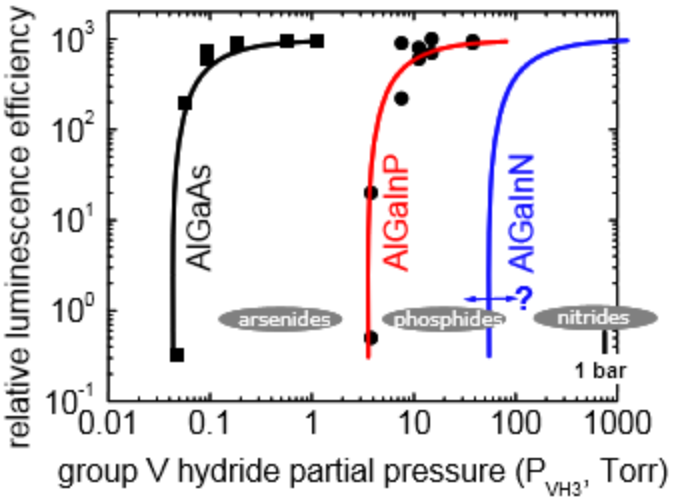

Figure 8: Quantum efficiency vs VH_3 partial pressure for different V-III semiconductor families, as well as the possibility of a III-Nitride curve

In 1991, Shuji Nakamura, working at Nichia Corporation, published a paper on a custom, two flow atmospheric reactor designed for GaN growth. The reactor had a novel two flow design, where nitrogen and hydrogen flowed normal to the substrate, and carrier gas, along with the precursors, flowed in from the side, parallel to the wafer's surface. The vertical flow was used to push the precursors towards the surface, allowing for uniform growth [28].

The designed reactor was an atmospheric pressure reactor, which produced the first GaN and GaN/InGaN LEDS and laser diodes. Although Nakamura does not specifically cite the reason for choosing to design the MOCVD system as an atmospheric pressure system, it seems likely that he considered the thermal stability of InN, as his InGaN work started out at temperatures around 500°C, with the intention of preventing InN dissociation during growth [29]. Nakamura began using higher temperature recipes with increased indium precursor flows as a result of work done by Yoshimoto et. al., at low pressure,

demonstrating that InGaN could be grown at higher temperatures, despite being above the dissociation temperature of InN [19]. Nakamura then went on to produce higher quality InGaN material, from similar recipes, than his counterparts, who were growing InGaN at low pressures (76 Torr).

CHAPTER 2: MOCVD ADDITIONS, MODIFICATIONS, AND DEVELOPMENT

2.1 Indium Alloy Capabilities

This work was done in the CFD-designed, superatmospheric MOCVD reactor at UNC Charlotte. At the start of this work, the reactor only had the capability to grow GaN and no growths above 1.5 bar(a) had been performed. To begin this work, it was necessary to add a metal-organic indium source, trimethyl indium, to the MOCVD system, all of the supporting hardware, and necessary additions to the control software. This is one of the five systems, outlined in the bottom left corner of Figure 9. A water bath was added, to control the temperature of the trimethyl indium, in the bubbler. Gas lines were fabricated and mass flow controllers (MFCs) were added to source nitrogen into the bubbler, to add "push" nitrogen, at elevated pressure, to the bubbler output for increasing the gas velocity of the MO to the reactor, and to enable protection and purging of these systems. Control and interface systems were added to the NI Labview MOCVD control program, as well as completing the recipe program for growth automation, which is critical for growth consistency and precision in multiple quantum wells (MQWs). The original design, for the gas delivery system can be seen in Figure 9.

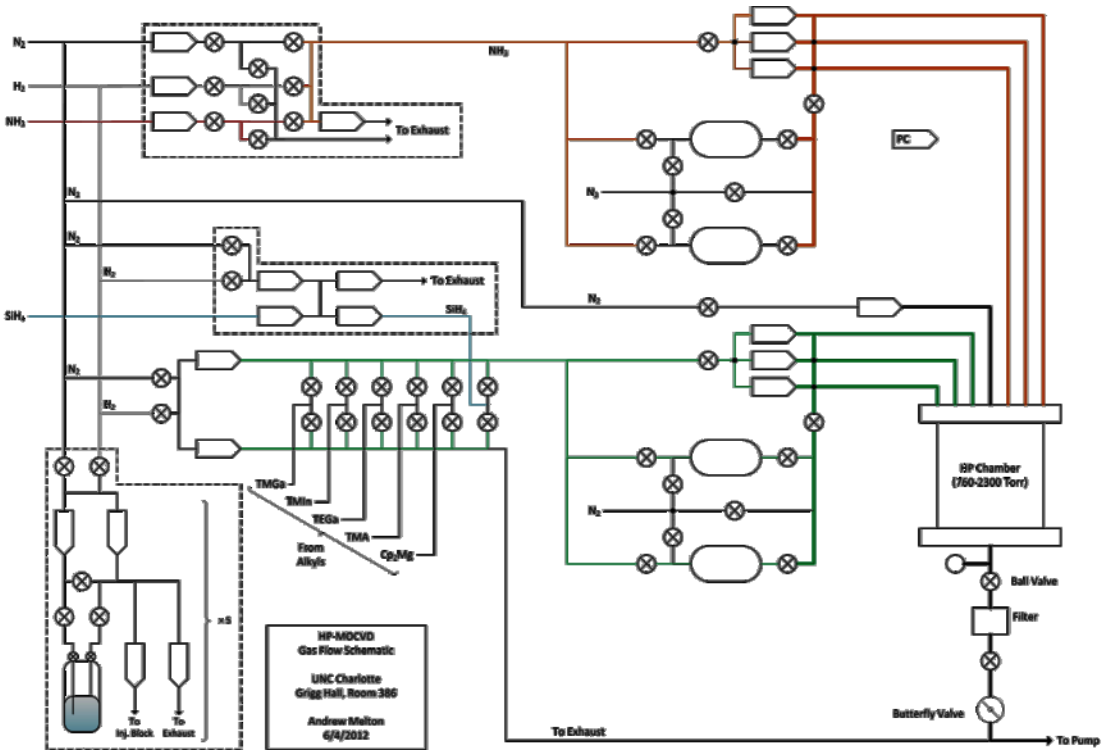

Figure 9: Original design for the HP-MOCVD gas delivery system

To keep this system working properly, it was necessary to provide means for keeping the metal-organics from sitting in the lines when not in use, condensing in the lines, and from backing up, all issues that are expounded in a pressurized system. Check valves (one-way flow) were added to the bubbler system and can be seen in Figure 10, to prevent back-flow. These have a turn on pressure of up to 0.07 bar, and were not a completely sufficient solution.

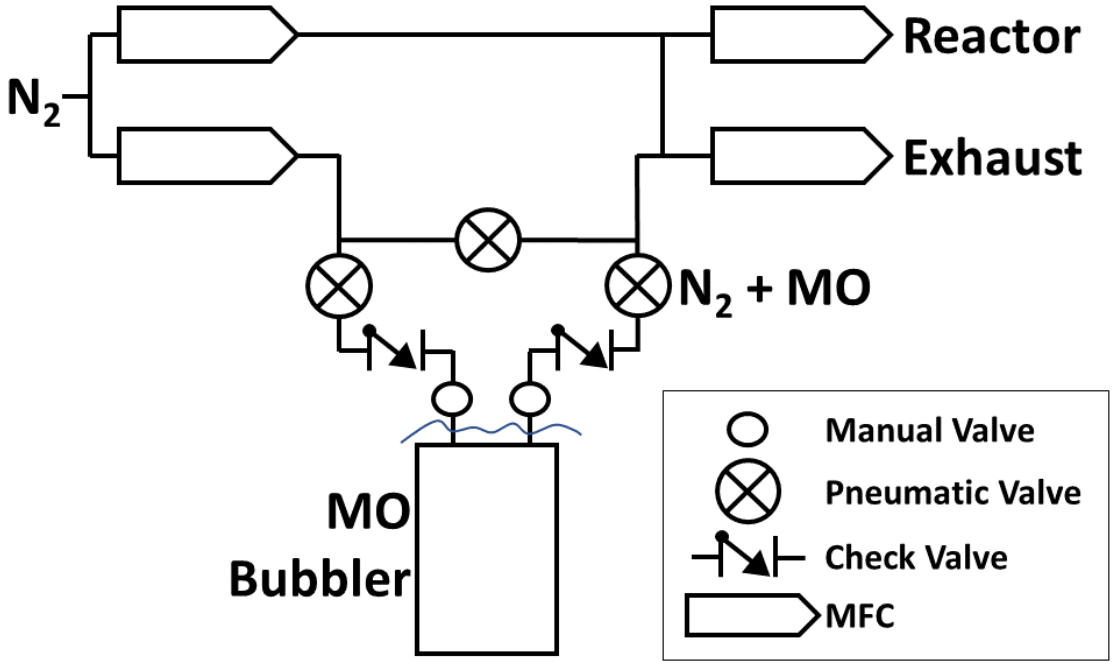

Figure 10: Diagram of MO bubbler and gas lines

A fill and purge process had to be developed to fully prevent equipment breakdown. Condensed and vapor-phase metal-organics were found in the gas lines around the MO bubblers, when only check valves and a simple vacuum process was used for clearing the lines, before and after growths. This was causing MFCs and valves to fail. A more complex method, of pressurizing and vacuuming the gas lines, was developed with significant success and can be seen in the "After Growth" section of APPENDIX A. Since instituting the new process, approximately four years and two months, there has not been a single MFC or valve failure in the bubbler lines.

2.2 Automatic Recipe and Control Software

Automatic temperature controls were added to the NI Labview control program. Because of the nature of the heater, an approximately 80mΩ tungsten resistive element, and the nature of our main substrates, GaN on Al_2O_3 templates, the temperature had to be ramped slowly. Quick temperature change would cause large changes in the current with respect to time, and possibly melt the heating element. The quick temperature change could also cause the GaN and Al_2O_3 to expand at different rates, due to their different thermal expansion coefficients, which would have the potential to crack the GaN layer, making it unsuitable for growths.

Several improvements were made to the NI Labview control program, with the last completed revision to date, being V1.6. This version is the version referenced in APPENDIX A: "HIGH PRESSURE MOCVD STANDARD OPERATING PROCEDURES". These improvements included the ability to automate temperature changes, including the rate of change, which was previously a completely manual process. The previously mentioned TMI bubbler controls were added as well. Several variables including temperature, temperature profiles, and the TMI gas delivery system were given the ability to be controlled by an automatic recipe, as well as other improvements. A general view of the main tab of the control GUI is seen in Figure 11.

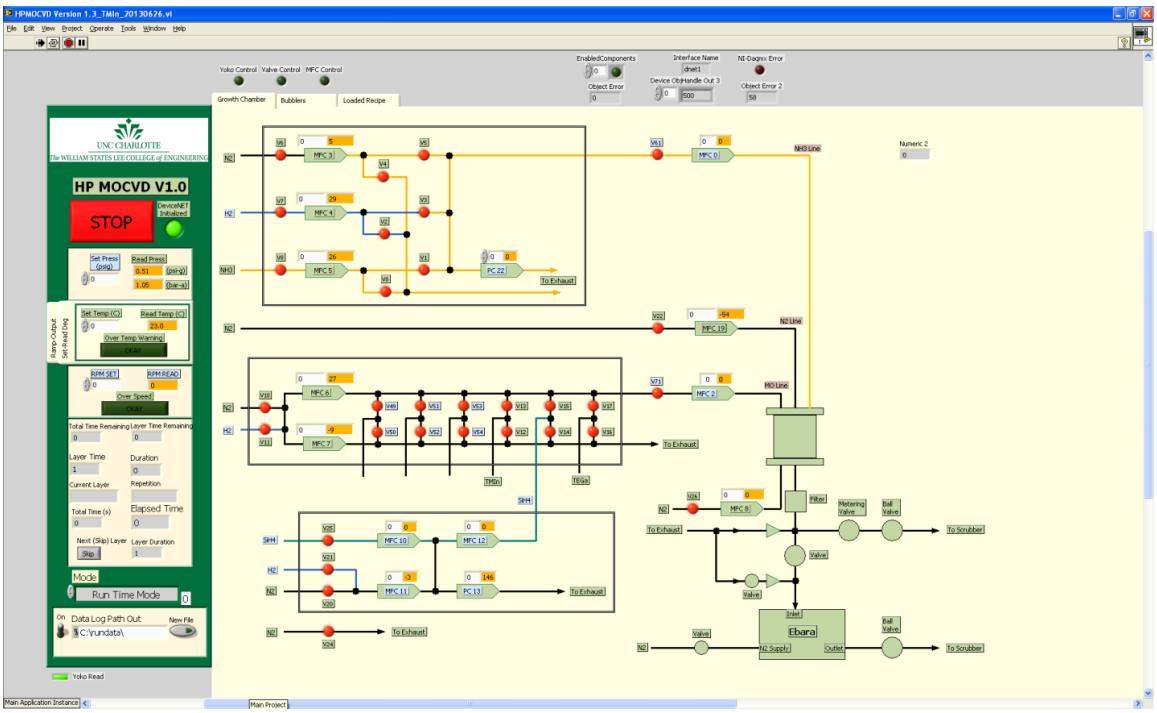

Figure 11: Main tab of the HP-MOCVD control software

The secondary program, the recipe creator program (HP-MOCVD Recipe Writer) was not functional at the start of this work. This program was completed, as part of this thesis, using its original software structure, so that source gasses, flow changes, and temperature changes could be automated. This allows for greater control and precision in growths, but, more critically, it achieves greater repeatability, which can be hard to obtain when manually changing valves and gas flow values used in a chemical reaction to create layers on the order of 3nm. This is the most important with device-like structures, such as multiple quantum wells, where manually switching parameters can lead to variability in the structure's layers. The main screen of the HP-MOCVD Recipe Writer can be seen in Figure 12 and the bubbler tab in Figure 13.

The HP-MOCVD Recipe Writer was designed to mimic the main control program, with several added variables, which were necessary for creating multiple layers (e.g. layer time). This way, a recipe could be created, like creating a sequence of system states. Each layer was saved as a row in a .csv file and could be imported into the main control program.

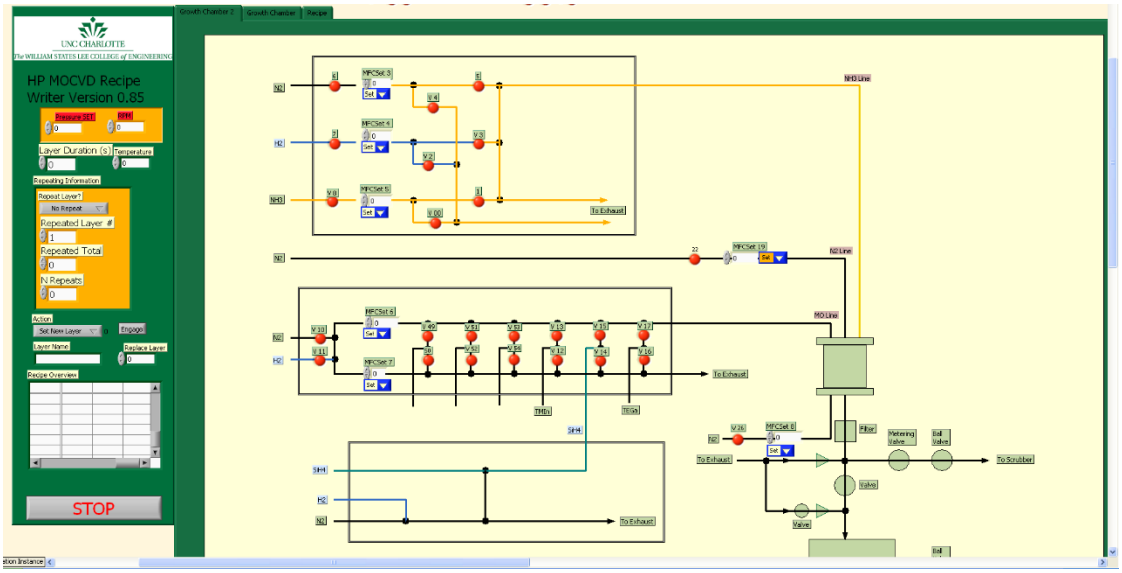

Figure 12: HP-MOCVD Recipe Writer main screen, showing the same layout as the main control program

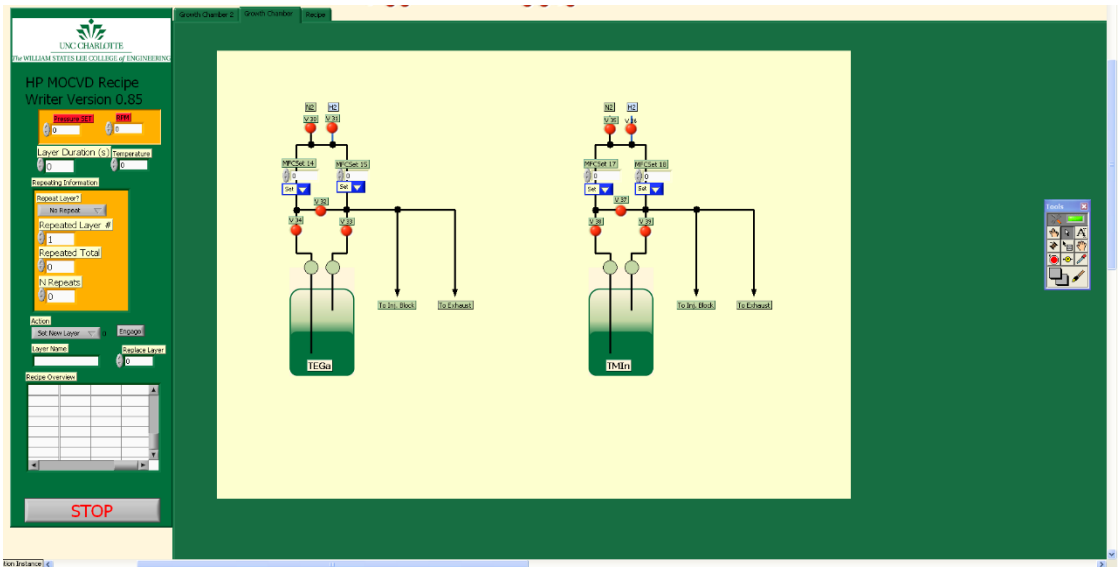

Figure 13: HP-MOCVD Recipe Writer bubbler tab

2.3 Reactor Inlet Gas Separator: Gas Delivery Turbulence Reduction

In addition to the changes that were necessary to complete the work, a physical change was made to reduce turbulence in the reactor. During the early stages of this work, which included running the CFD simulations, developed in the original reactor design work, it was noted that one of the assumptions in the CFD model was not matching the fabricated reactor. In the CFD model, all three separated gas flows were entering the reactor at the same velocity and angle. However, ratio of the three areas did not match the ratio of the volumes/minute that were flowing through them. Since the separator was fabricated with an approximate 1:1:1 ratio, and the ratio used was on the order of 18:5:18, one section of flow was coming in at a significantly slower velocity. When this part, outlined in Figure 14 was changed, an immediate improvement in sample quality was seen.

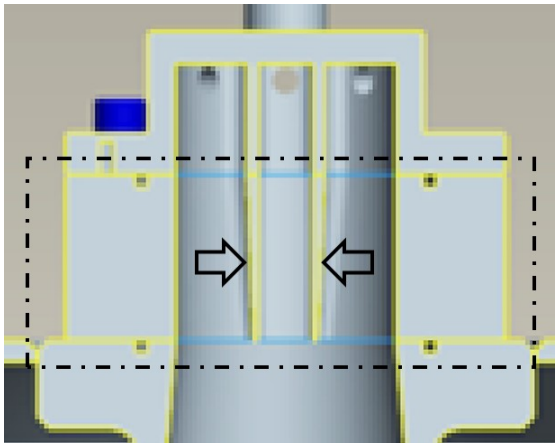

Figure 14: Gas separator insert, later refabricated to match flows and keep design consistent with simulation(s)

CHAPTER 3: EXPERIMENTAL METHODS

3.1 InGaN Thin Film Studies

Any research must start somewhere, and due to the nature of this project, which involved a high pressure III-Nitride MOCVD reactor with no previous ternary alloy development, no historical data was available. Also, due to the fact that high pressure MOCVD is relatively new and therefore not widely studied, there is not much data on super-atmospheric processes. When this work began, Dr.Dietz's group at Georgia Tech was the other main group studying the subject and they are pulse injecting pressurized precursors into a small horizontal reactor, one at a time, with pulse lengths determined by optical interferometry [30] [31]. Because the precursors are not diffusing through the boundary layer and reacting simultaneously, the chemical data, such as V:III and In:Ga ratio, is hard to make correlations with. The only III-Nitride data from the UNC Charlotte reactor was from preliminary GaN growths, grown at 200-300°C above typical InGaN process windows. Therefore, the initial starting point for the researching high pressure MOCVD of InGaN was taken from the preliminary GaN growths and literature employing low and atmospheric pressure processes [8] [17] [29] [32] .

3.1.1 Group-III Flux Investigation

Initial ternary experimentation was in the area of the group-III fluxes. Temperature, group-III molar flux, which is directly related to the growth rate of the material, and In:Ga ratio were focused on. This subset of samples was grown at 1.5 bar(a) and all quoted temperatures are referencing the substrate temperature. The samples were grown on GaN on Al_2O_3 templates and a GaN cap layer was grown on top of the film to prevent indium dissociation from the crystal before the substrate can cool after growth stops. The cap was determined to be necessary and verified, by experimentation.

The first subset consisted of three samples, HP11, HP13, and HP17. The recipe for HP17 was performed twice, once for HP16 and once for HP17, although most data was taken from HP17. In this series of growths, temperature was modified, then group-III flux and growth thickness were modified.

The initial recipe was used on sample HP11, which was then modified to examine sample differences versus input differences. In addition to the conditions already stated, the initial recipe had a group-III molar flux of 59.8 µmol/min, a V:III ratio of 7,562, an In:Ga ratio of 3:1, and a substrate temperature of ~630°C.

The temperature in the recipe for HP11 was lower than reports in low pressure growths. Because of this, in the recipe for HP13, the substrate temperature was increased by 120°C. For sample HP17, the group-III molar flux was decreased from 59.8 µmol/min to 15 µmol/min, as well as a decrease in growth time from 11 minutes and 25 seconds to 6 minutes and 25 seconds. The decrease in growth time was to ensure that the film did not grow beyond its critical thickness. These samples were then analyzed with XRD, PL, SEM, and EDAX.

3.1.1.1 Follow Up Experiment: Lower In:Ga Ratio, Higher Temperature

After the results of HP11- HP17, the optimization trend that they outlined was pursued further. The results had indicated that the In:Ga ratio was still too high, even though it was very similar to In:Ga ratios reported for low pressure growths. The results of HP11 – HP17 also indicated that an increase in temperature could help bring the growth environment to one that is chemically favorable to growing crystalline III-Nitrides.

To investigate and support this hypothesis, growths with similar recipes, were planned and performed, with slight modifications. This report will focus on one of the first samples, HP23. The recipe for HP23 was the same as HP17's, with a decreased In:Ga ratio and an increased growth temperature. The temperature was set to approximately 780°C on the substrate, which was 30°C higher than HP17. The growth was completed at 1.5 bar(a), with the same V:III ratio of 30,248, but the In:Ga ratio was lowered from 3:1 to 3:5. The structure was grown on a GaN template, and the structure was an InGaN active layer with a GaN buffer and cap layer. Each layer was approximately 20nm thick. EDAX, PL, low temperature PL, and XRD were used to characterize HP23.

Excluding a single growth, all growths, from this point forward, used a maximum In:Ga ratio of 3:5 (37.5% TMI) and the majority used 1:3 (25% TMI) or less. All of the growths that produced luminescing InGaN (and therefore were further characterized) had indium concentrations in the 9-15% range, which further demonstrates that InGaN can be grown superatmospherically, using In:Ga ratios approximately a single order of magnitude below the standard for low pressure processes.

3.1.2 Photoluminescence and Growth Temperature Investigation

The InGaN processes had a lowered In:Ga ratio, at this point in the research. Some of the low pressure, academic reports had included lower temperature growths, to attempt higher indium content, in the InGaN layers. Significant room temperature PL had not yet been achieved in this work's samples, so this series of experiments was specifically performed to investigate the effects of temperature on photoluminescence.

The hypotheses, for this experiment, were all based upon the role of temperature, in the growth process. Two of the main hypotheses, driving the investigation into temperature, are the possibility that carbon is getting incorporated into the crystal lattice (undesired impurities), and that the structural quality of the crystal lattice is compromised by low mobility, from the relatively low temperatures. The hypothesis on carbon incorporation is that there is incomplete pyrolyzation of the precursors and pyrolyzation happening too close to the substrate, both causing carbon to reach the surface and get incorporated into the lattice. The experiment started at the relatively lower temperature of ~700ºC and raised the growth temperature, in HP39 and HP40 respectively, to ~775ºC and ~800ºC to see what changes the would come about, especially if it would bring about room temperature PL.

HP38, HP39, and HP40 were grown across a range of temperatures, from ~700ºC to 800ºC. The nominal recipe, for this experiment, was a 1:5 In:Ga ratio, a 45,101 V:III ratio, and the pressure was set at 1.5 bar(a). These samples were all grown on VEECO u-GaN templates. The main method of characterization of the samples was with PL, as Secondary Ionization Mass Spectroscopy (SIMS) was not available, to my knowledge, to

reliably measure the carbon content. PL is a secondary measure of quality, in this respect, but useful to show changes in the samples.

3.2 Multiple Quantum Well Studies

3.2.1 Buffer Layer Investigation

3.2.1.1 Initial Buffer Layer Growths

In the interest of moving towards device-like structures, the research moved from film growths to multiple quantum well (MQW) growths. There are many options in the design of a multiple quantum well structure, but we started with a base structure and concentrated on optimizing the MOCVD grown InGaN material instead of the design of the multiple quantum well structure. However, the effect of growing a homogenous (GaN on GaN) buffer layer before the structure itself was not known.

In the beginning of this research, it was thought that growing a homogenous buffer layer would be unnecessary, due to the use of GaN templates These templates have HVPE grown GaN, on Al_2O_3. However, analysis showed that the most recent samples had some roughness in their surfaces. This brought about the investigation into the buffer layers.

A series of growths were performed, with different buffer layer recipes. There were two without buffer layers, three with high temperature buffer layers, and one with a low temperature buffer layer. The sample numbers and their correlated buffer layer property can be seen in Table 1.

Table 1: Sample numbers and buffer layer parameters

Sample	Buffer Layer Temperature
HP52	High Temp: 1100ºC$_{tc}$, 980ºC$_{substrate, estimated}$
HP53	High Temp: 1100ºC$_{tc}$, 980ºC$_{substrate, estimated}$
HP54	None
HP55	None
HP56	Low Temp: 930ºC$_{tc}$, 800ºC$_{substrate, estimated}$
HP57	High Temp: 1100ºC$_{tc}$, 980ºC$_{substrate, estimated}$

3.2.1.2 Buffer Layer DOE

After the initial investigation into the buffer layers, a two-parameter design of experiments was run on the high temperature buffer layers. The two parameters were temperature and thickness. It had already been found, that ~1060°C, which is 1100°C at the thermocouple, produced better results than the ~810°C, 930°C at the thermocouple, so the leading question was whether the temperature should be increased further. The secondary question was how a thin layer, approximately 4-6 nm, compared to the approximately 25nm layers that were being grown, and if the effect was one similar to the effect of a thin AlN buffer layer between sapphire and GaN.

Four samples were grown, two at 1200°C, and two at 1100°C, referencing the thermocouple temperature. At each temperature, two samples were grown, one for 2 minutes (~5nm) and one for 10 minutes (~25nm). The buffer layer temperature and thickness DOE can be seen in Table 2.

Table 2: Buffer layer temperature and thickness DOE

	~5nm (2min)	**~25nm (10min)**
1200ºC$_{tc}$	HP61	HP62
1100ºC$_{tc}$	HP64	HP63

3.2.2 Photoluminescence over Pressure

This experiment was done to see the effects of increasing the pressure in the reactor for growths. There are two theories that are expected to come into play here, the increased stabilization of the ternary alloy, as the MacChesney data indicates, and an increase in the IQE, as data from Dr. David Bour and Dr. Edward Stokes indicates, should happen as the N partial pressure increases [13] [26] [33] [34]. For this experiment, a series of MQWs were grown, at increasing pressures. The respective volumetric flow of the group-V precursor was kept constant to obtain an increase in group-V partial pressure with the increase of total reactor pressure.

The group-III molar flow was kept constant throughout the experiment. Reductions in carrier gas flows through the bubblers and temperatures in the bubblers was necessary to achieve this. By keeping the group-III molar flow constant and keeping the volumetric flow of the group-V precursor constant, the V:III ratio was increased as the pressure increased. This is the one extraneous change that was allowed during this experiment.

The increase in the V:III ratio was not expected to have a large impact on the outcome of the growths, although it could have some effect. Because there is adequate group-V precursor to participate in the reaction, and the experiment increases the V:III

ratio, no effect from the perspective of inadequacies in the reaction is expected, as was seen in the first attempt to use known, low pressure processes. However, the increase in group-V atoms on the surface could affect the kinetics of the group-III atoms, most significantly by reducing their surface mobility [35] . This has been shown to change growth modes from island growth to step growth [8], but the samples should already be in step growth mode, even in the lowest V:III ratio employed in this experiment. The other effect that could happen, is a widening of the FWHM, due to inhomogeneous composition, with respect to the group-III atoms. It has also been shown that reducing the group-III mobility, through an increase in the V:III ratio, can lead to the inability of the group-III atoms to travel enough distance across the surface to achieve compositional equality across the sample [18].

These growths were all with the structure seen in Figure 15 and their parameters can be seen in Table 3.

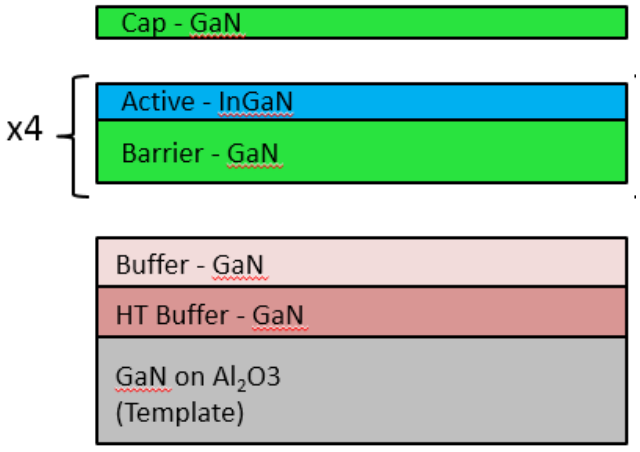

Figure 15: MQW structure for IQE vs pressure experiments

Table 3: Pressure experiment samples and respective changed parameters

Sample	Pressure	P_{NH3}	V:III Ratio
HP76	1.5	0.55	90k
HP78	2.0	0.73	120k
HP79	2.5	0.91	150k

Referring to the previously mentioned heater, susceptor, and thermocouple design, the system is somewhat susceptible to undetected changes in substrate temperature. This can be caused by things such as a height shift in the susceptor alignment.

CHAPTER 4: RESULTS AND DISCUSSION

4.1 InGaN Thin Film Studies

4.1.1 Group-III Flux Investigation Results

The three samples, HP11, HP13, and HP17 were characterized with XRD, EDAX, SEM, and PL. None of the photoluminescence data showed room temperature luminescence and 78°K data was not taken for these samples. However, the SEM, XRD, and EDAX data was in agreement, and relevant.

When removed from the reactor, HP11 had a visible mix of silver and black on the wafer. The wafer has a metallic appearance, compared to the approximately white, but somewhat transparent, color of the GaN template that the material had been grown on. The silver and black colors were somewhat swirled, although this is not thought to be of any significance.

An SEM scan of HP11 was taken. It showed a very rough surface, with many "holes" in it. The image was somewhat reminiscent of pumice stone or lava rock, which can be seen in Figure 16. In the SEM image, holes in the growth surface can be seen, as large as 2x5μm.

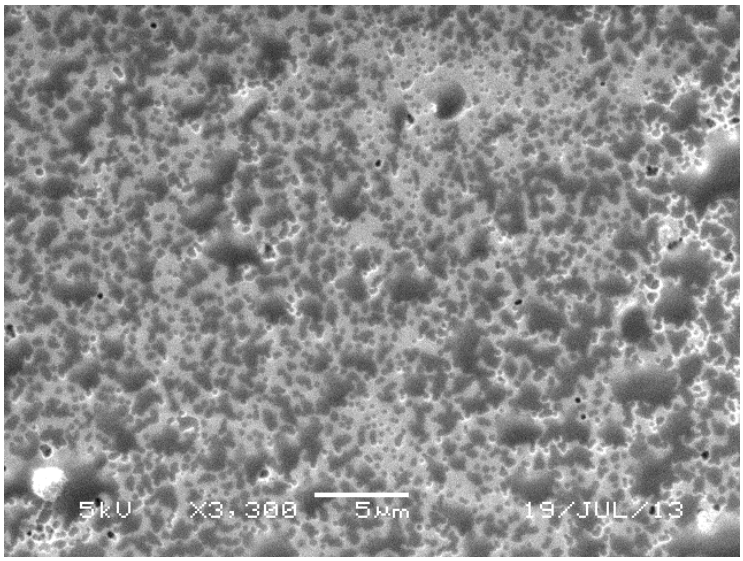

Figure 16: SEM image showing a pumice-like surface on HP11

To compare the surface of the final growth, SEM was used on HP16, which was grown with the same recipe as HP17, the main sample measured for this experiment. An SEM image of HP16 can be seen in Figure 17. The recipe used for HP16, inferring HP17 as well, produced a significantly smoother surface. Two inclusions can be seen in this image, one of them is on the order of 3.5µm.

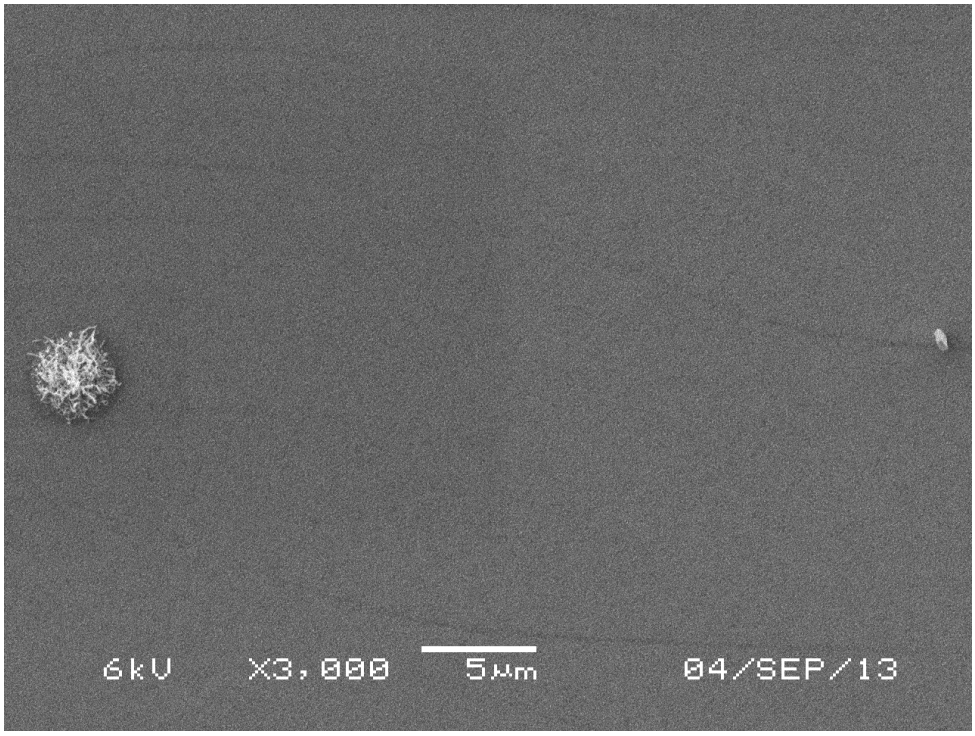

Figure 17: SEM image, showing a smoother surface on HP16, grown with HP17 recipe

This indicates that the increase in temperature, decrease in group-III flux, and the decrease in thickness improved the surface quality significantly.

X-Ray Diffraction was completed for all three samples, HP11, HP13, and HP17. The results, including normalized intensity of the curves for comparison, can be seen in Figure 18. For the normalized curves, the original data is included as a dotted line, for reference.

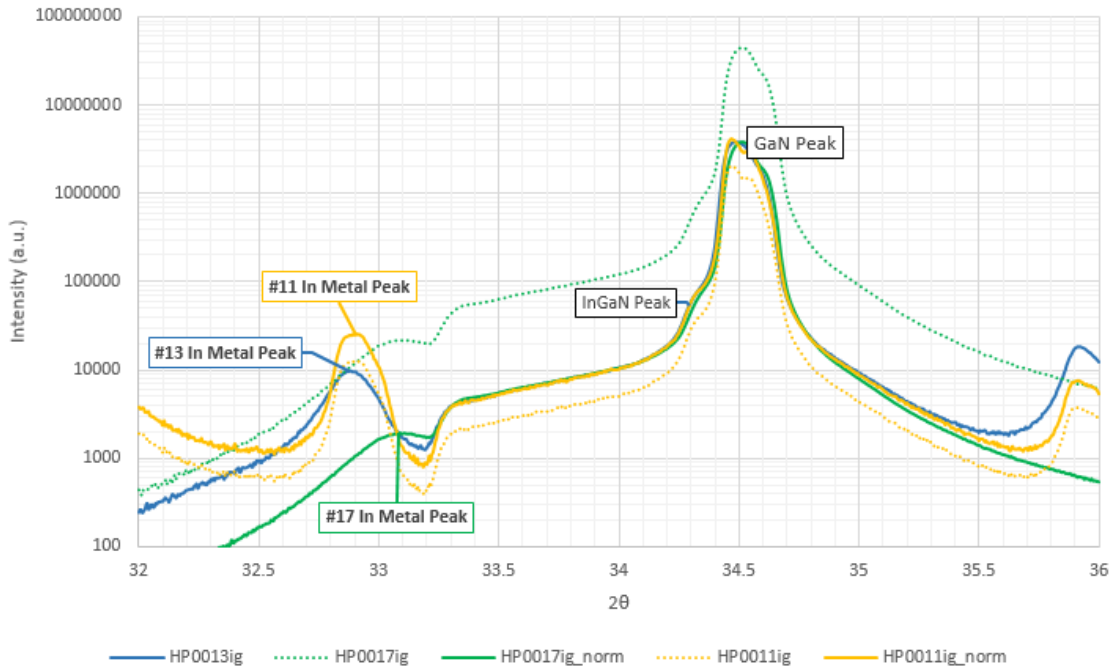

Figure 18: X-Ray diffraction of HP11, HP13, and HP17, showing decreasing In peaks

There are three main peaks in the XRD plots, which have been labeled for quick reference. These include an indium metal peak, a GaN peak, and a possible InGaN peak, although it may also be a template artifact. A fourth peak can be seen around 35.9º, which is due to the AlN buffer layer and proprietary buffer layers in the template. Several significant data points can be extracted from the XRD data.

The first is that the indium metal peaks are decreasing with each growth. The changes made to reduce the indium metal peaks were increasing the substrate temperature by 120°C between sample HP11 and HP13, and between sample HP13 and HP17, the total group-III flux was reduced by 44.8 µmol/min and the film was only grown for 6 minutes and 25 seconds instead of 11 minutes and 25 seconds. The In:Ga ratio was held constant. Using the normalized plots, the intensity of the indium metal peaks can be seen in Figure 19.

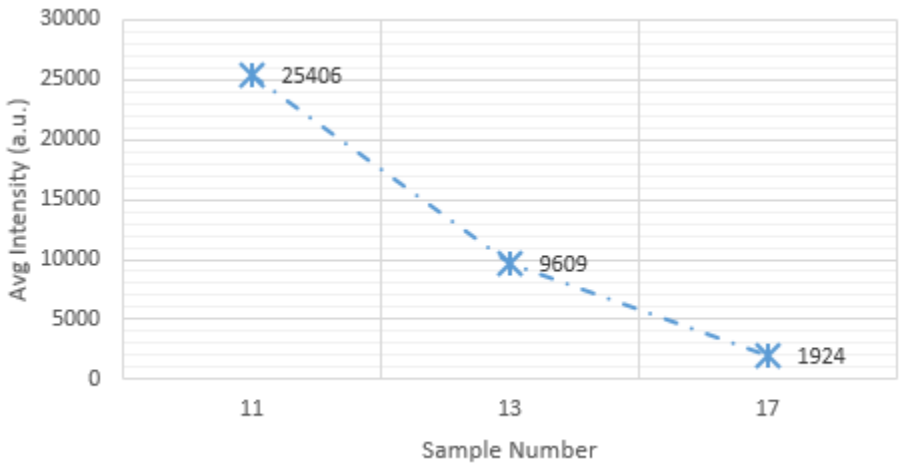

Figure 19: Indium metal peak XRD intensities for HP11, HP13, and HP17

There was a significant decrease in the indium content, between HP11 and HP13, with the temperature increase. There was a 37.8% decrease in excess indium content, with an increase in growth temperature of 120ºC. This is a slope of -0.32% indium content per degree Celsius. This shows that temperature is a significant factor in the amount of indium that is remaining on the surface. This finding is supported by multiple works in low and atmospheric pressure MOCVD of InGaN, where certain process conditions, especially temperature could cause indium metal droplet formation [17] [18] [36]. Keller et. al. using MOCVD at atmospheric pressure, plotted samples on a 2-axis temperature vs NH_3/TMIn graph, which could be split, approximately linearly, into two regions of growth. The region with lower temperatures and lower NH_3/TMIn was indicated as a region of growth with indium metal droplets [17].

In Figure 19, different mechanisms are at work. Both led to an improved chemical balance at the substrate surface. The proposed mechanism at work between HP11 and HP13 is the increase in temperature, giving more thermal energy to the reaction. This

should have caused more efficient pyrolyzation of NH_3, making more N atoms available for surface reactions. This also should have increased the rate of indium dissociation from the substrate, since the increase in temperature increases the thermal energy of the atoms, coupled with the high vapor pressure of indium [18]. This makes it easier for them to break bonds with the lattice and the self-attracting property of indium metal.

Although epitaxial crystal growth was not achieved in HP11 and HP13, it was shown that the indium content has a large dependence on temperature, in this process window. Although most of this is excess indium, it is possible that indium content, in the ternary alloy, will have a significant temperature dependence. If true, this would make temperature one of the process values to investigate, when creating recipes for specific indium content in the ternary alloys.

In the second stage of the experiment, the total indium flowed into HP17 was reduced to 14% of HP13. The total In flow was reduced in two ways, first the growth height was reduced by 44%, and the indium precursor flow rate was reduced by 75%. If all physical processes produced a 1:1 reaction, with these changes, the indium content in HP17 would be 14% of HP13 (Eq'n 2). Since there was a significant indium metal peak in the XRD scan of HP13, it could be expected that most of the In reduction would come from the excess indium, unless the flow was reduced too much. Based on the indium peak intensities, in the XRD scans of HP13 and HP17, the excess indium content in HP17 was approximately 20% of HP13 (a reduction of 80%). This was not exactly the number expected, but close. However, when the indium precursor flow was reduced, the In:Ga ratio was held constant. This means the Ga precursor flow was reduced to 25% of its

previous flow as well. This could account for part of the In content not changing in a 1:1 fashion.

The reduction of indium precursor flow should have directly impacted the excess indium content, by putting less indium per second into the attempted crystal growth reaction. The improvements related to the reduction of total indium in the sample (growth thickness) is expected to be related to the critical thickness and reports that indium metal formation can reach a critical point and overtake the crystal growth process [37] [38].

$$In_{total} = In_{flow} * T_{growth} \quad \text{Eq'n 1}$$

$$In_{totalHP17} = In_{totalHP13} * \frac{11.21\ \mu mol/min}{44.85\ \mu mol/min} * \frac{6.42\ min}{11.42\ min} = In_{totalHP13} * 0.14 \quad \text{Eq'n 2}$$

The reduction in group-III flux affected the growth in three ways. It increased the V:III ratio, making more nitrogen available for each group-III element; decreased the overall group-III flux, but specifically the indium; and decreased the growth rate, giving growth processes more time to complete. The increase in the V:III ratio, through group-III flux reduction, led to a reduction in the amount of group-III atoms available per group-V atom. This directly helped to minimize the excess indium found on the surface.

One of the hypotheses was that the metallic surface of HP11 was caused by more group-III atoms reaching the substrate, than could be incorporated into a crystal lattice. This would result in deposition, instead of epitaxy. Reduction of the group-III flux, would directly reduce the excess indium, on the surface.

The decrease in growth rate is thought to have assisted in the surface quality, as well as the lack of excess indium metal, as it would give the atoms more time to arrive at lattice sites and allows an increased indium dissociation rate. This is because faster

growth rates “trap” some of the indium that would have dissociated with the currently growing layers. The slower growth rate has less trapping material on top of the indium that is trying to dissociate allowing more indium to dissociate from the substrate.

Using the EDAX detector, fitted in the SEM, composition scans were made of HP11 and HP16, to confirm the results shown above. The scans were made at several places across the wafer and significant variation was seen in HP11. The data from the scans can be seen in Table 4 and 5. In addition to the fact that HP11’s X-Ray fluorescence data shows a relatively high standard deviation across the sample, it can quickly be seen that HP11’s group-III content is far exceeding the group-V content, which should have, approximately, a 1:1 content ratio (N:In+Ga). The In:Ga ratio, displayed as In/Ga,is also quite high, confirming excess indium and excess total group-III deposition on HP11.

Table 4: X-Ray fluorescence data of HP11, revealing excess indium deposition

	N (% Comp)	Ga (% Comp)	In (% Comp)	O (% Comp)	**Meas III/V**	**Meas In/Ga**
Center	16.53	10.12	66.17	7.18	**4.62**	**6.54**
Center2	18.87	10.27	70.86	0	**4.30**	**6.90**
Flat Edge	33.70	8.19	58.11	0	**1.97**	**7.10**
Flat Edge2	9.72	11.26	79.02	0	**9.29**	**7.02**

Table 5: X-Ray fluorescence data of HP16, showing improvement in composition

	N (% Comp)	Ga (% Comp)	In (% Comp)	O (% Comp)	**Meas III/V**	**Meas In/Ga**
Smooth-a	33.63	38.17	13.34	4.72 +C(10.15)	**1.53**	**0.35**
Smooth-b	37.29	41.80	15.71	5.18	**1.54**	**0.38**
Smooth-c	38.56	46.11	10.38	4.95	**1.46**	**0.23**
Object-a	22.65	27.02	46.09	4.24	**3.23**	**1.71**
Object-b	13.36	13.22	69.06	4.37	**6.16**	**5.22**

HP16's X-Ray fluorescence data shows a significant decrease in the group-III to group-V ratio, on the sample. There was also a significant decrease in the In:Ga ratio, on the sample. This confirms the XRD data, showing an improved composition with the temperature and group-III flux changes.

The SEM data showed that there were two inclusions/objects in the area scanned, approximately 36μm apart. These objects were scanned with X-Ray fluorescence as well, and were found to have excess group-III and indium deposition. With the overall sample having significantly less group-III and indium, it appears that some droplets, consisting of mostly indium metal, were able to form on the surface.

The maximum, minimum, and average group-III content and the average In/Ga and group-III/group-V content, for HP11 and HP16, can be seen in Table 6.

Table 6: Minimum, maximum, and average group-III content. HP16 does not include objects.

	Group-III atomic %			Content Ratios	
	HP11	HP16		HP11	HP16
Average	78.5	55.17	Average In/Ga	6.89	0.32
Maximum	90.3	57.51	Average III/V	5.04	1.51
Minimum	66.3	51.51			

4.1.1.1 Follow Up Experiment: Lower In:Ga Ratio, Higher Temperature Results

Sample 23, produced clear, measurable results. EDAX, PL, low temperature PL, and XRD were used to characterize sample 23. Although compositional data could not be derived from the EDAX due to it probing to an unknown depth in the wafer and the fact that the top GaN layer would be included in the measurement, it could be used to confirm or deny the presence of indium, gallium, and nitrogen, as well as other possible contaminates.

Industry grown GaN on Al_2O_3 templates were scanned for comparison. An HVPE grown template, from Kyma Technologies, Inc and two MOCVD grown templates, from VEECO Instruments, Inc, were scanned. These were compared with the data from HP23. The EDAX data, seen in Table 7, confirmed that indium was in all areas of the wafer. It also showed that the group-III/group-V was now in line with industry GaN templates. It can also be noted that the measured carbon content is in line with the industry MOCVD templates, while the HVPE templates did not produce any measured carbon content.

Table 7: HP23's X-Ray fluorescence results, showing data similar to industry grown templates

	N (% Comp)	Ga (% Comp)	In (% Comp)	O (% Comp)	**Meas III/V**	**Meas In/Ga**
HP23-a	34.40	48.48	2.15	0 +C(14.97)	**1.47**	**44.37e-3***
HP23-b	34.74	45.88	0.45	1.2 +C(17.73)	**1.33**	**9.85e-3***
Kyme-T4	42.38	57.62	0	0	**1.36**	
VEECO-pc	35.45	48.08	0	0 +C(16.46)	**1.36**	
VEECO-T11	36.91	51.24	0	0 +C(11.84)	**1.39**	

The room temperature PL results were poor; there was a small luminescence peak in the 430nm region. It was several orders of magnitude lower than the GaN and yellow band peak intensities, indicating poor optical quality in the growth. While taking PL at 78k, using a cryostat and liquid nitrogen, a definable peak formed at ~433nm. The room temperature and 78k PL can be seen in Figure 20.

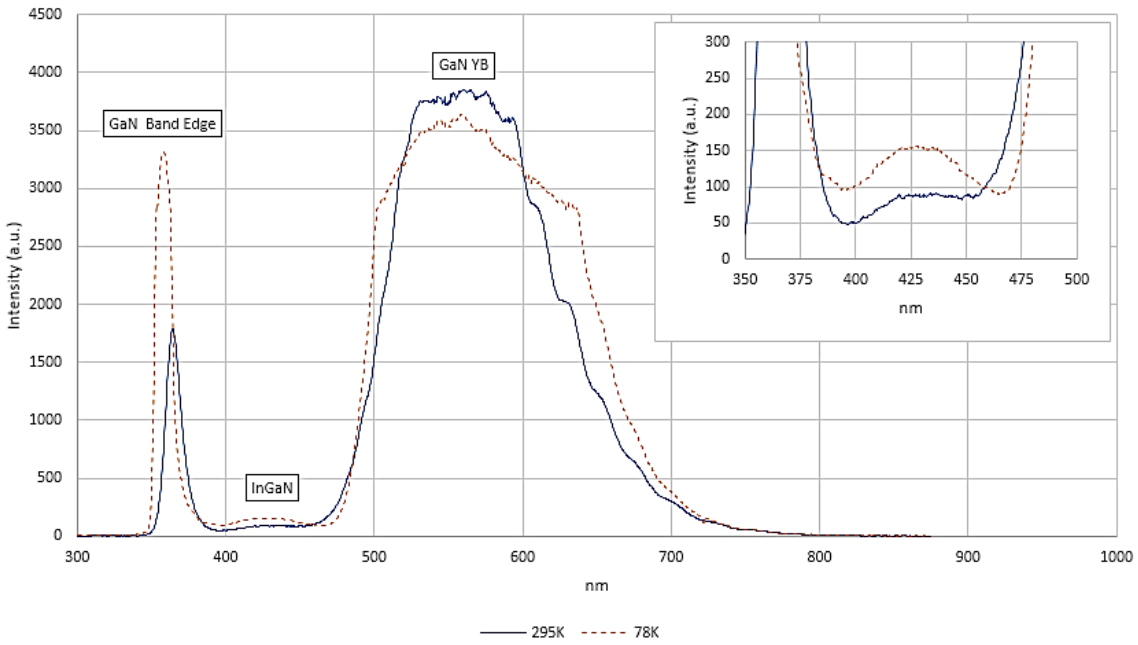

Figure 20: HP23's 78.5°K and 295°K PL spectrums, showing a small InGaN peak. Inset: close up of InGaN peak

A 2θ-ω scan was taken with the XRD instrument and the XRD results showed a significant InGaN peak and a possible second peak, which can be seen in Figure 21. The XRD results confirm that crystalline InGaN was grown. The highest composition peak is at 33.7142°, which, using Vegard's law without a bowing parameter, corresponds to 13.4% indium incorporation [39]. This composition, using a bowing constant of 1.6, corresponds to an energy of ~2.87eV, which is also where the small PL peak was found, meaning the measurements are in agreement.

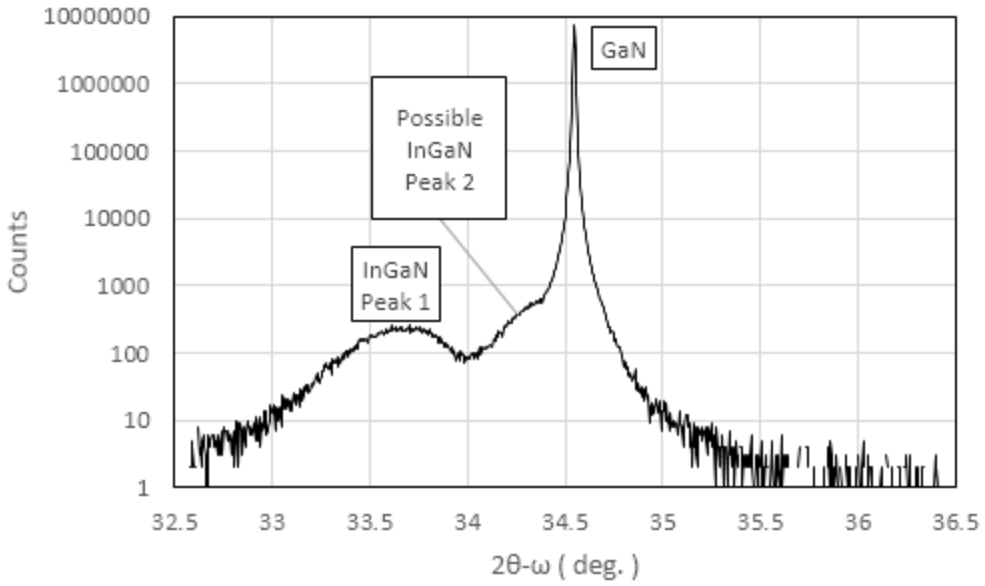

Figure 21: 2θ-ω XRD scan of HP23, showing InGaN diffraction peaks

HP23 demonstrated that the high In:Ga ratios reported in many low pressure processes, are not necessary, with these recipes/process windows. HP23, and all of the samples grown before HP23, were grown at 1.5 bar(a). The temperatures, in the growths, covered a range, but are within the reported values of low temperature growths. When comparing the In:Ga ratio and the calculated In content, the TMI flow is significantly reduced, with HP23 using 37.5% of the Group-III flux being and In precursor, but still obtaining 13.4% In, in the final sample.

Excluding a single growth, all growths from this point forward (HP24 – HP90), used a maximum In:Ga ratio of 3:5 (37.5% TMI) and the majority used 1:3 (25% TMI) or less. All of the growths that produced luminescing InGaN (and therefore were further characterized) had indium concentrations in the 9-15% range, or greater, which further demonstrates that InGaN can be grown superatmospherically, using In:Ga ratios

approximately a single order of magnitude below the standard values for low pressure processes.

The mechanism that is thought to be allowing this, comes from the previously mentioned work of MacChesney et.al., where it was found that the binary, InN, is stable at increased temperatures when grown with increased pressure. Since InGaN is usually grown above InN's stable process window, most of the In-N bonds are broken and the indium is dissociated, or the indium is never incorporated into the crystal at all, causing poor indium incorporation efficiency. It is proposed, that growing at elevated pressures, such as the current growths at 1.5 atmospheres, has stabilized the material enough to significantly affect the dissociation rate and increase the stability of the ternary alloy.

4.1.2 Photoluminescence and Growth Temperature Investigation Results

HP38, HP39, and HP40 were grown with increasing temperatures of ~700ºC, 775ºC, and 800ºC, respectively. Room temperature and 78K photoluminescence spectra were taken. Additionally, XRD data was taken for HP40. The photoluminescence data can be seen in Figure 22.

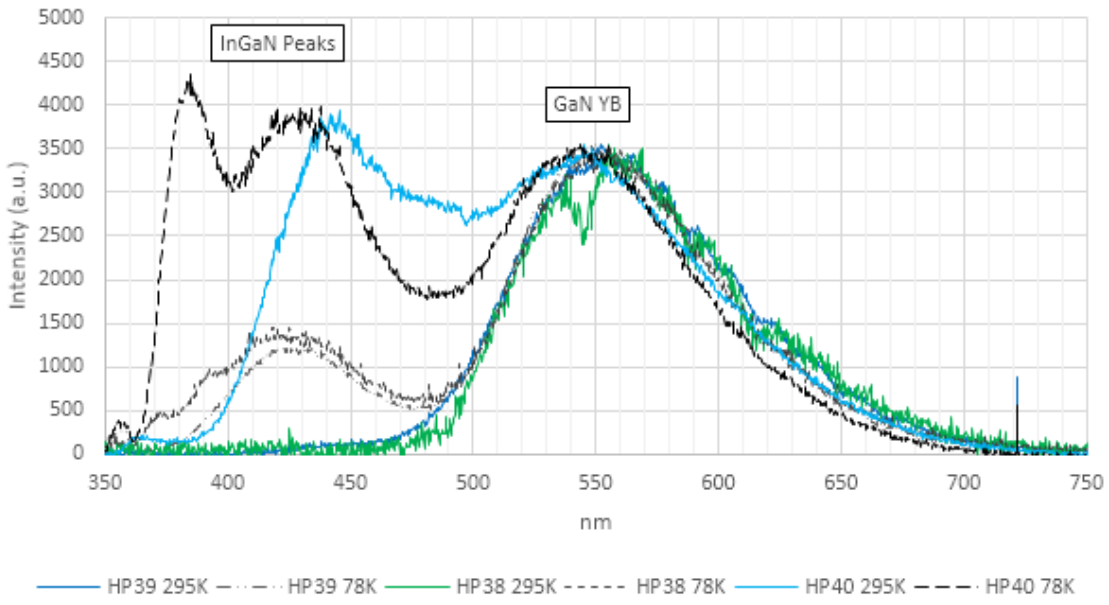

Figure 22: PL of HP38, HP39, and HP40, showing increased intensity with growth temperature

The room temperature PL spectra, for HP38 and HP39, do not show any InGaN band edge luminescence. HP40, however, shows a significant increase PL intensity, with the InGaN band edge luminescence slightly higher than the yellow band luminescence. It has a peak at ~440nm, with a very wide FWHM. The shape and width of the FWHM indicate that the composition of the InGaN active layers is probably not completely homogeneous. This would agree with other reports of inhomogeneous indium distributions in the active layers of quantum wells [40].

The 78K PL spectrums give a better look at the progress through the temperature increases, since there is PL in each growth. The approximate peaks values can be seen in Figure 23.

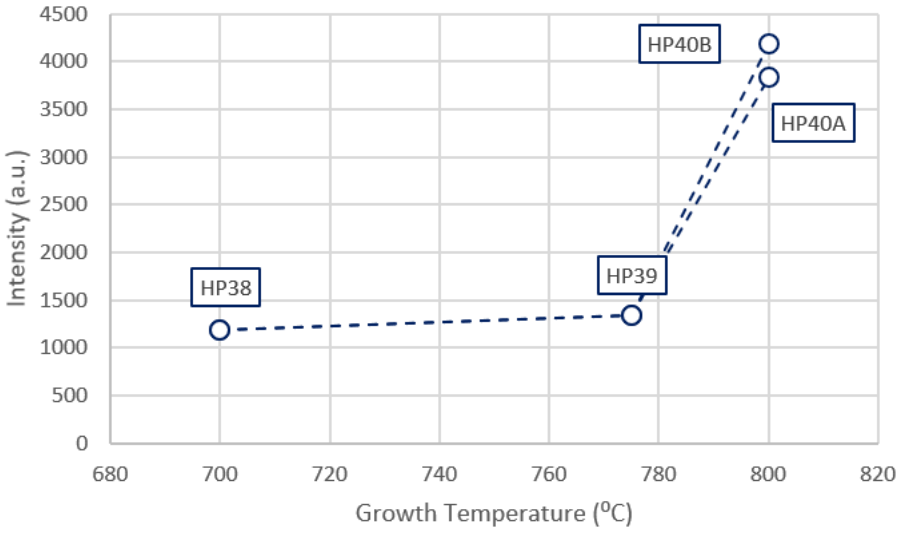

Figure 23: Graph, showing increase in 78K PL intensity with growth temperature

The increase from ~700ºC to 775ºC was only ~5.6% of the PL intensity increase from ~775ºC to 800ºC. This is a significant non-linearity. There are multiple possibilities to what the dominant physical mechanism causing the PL is. However, this work did not go into a deep enough investigation to be able to determine whether it is structural, related to impurities and defects, or otherwise.

It can also be noted, from the PL spectrums, that a second peak appeared in the 78ºK spectrum, from the final growth. Based on the PL alone, it appears to be a second, distinct composition of InGaN. This could be an effect due to the lattice constant constraint, at the GaN/InGaN interface. It could also be related to an incomplete nucleation layer, causing 3-D growth instead of 2-D epitaxy.

The x-ray diffraction of HP40 confirmed the presence of InGaN. In Figure 24, the XRD plot can be seen and a second peak, around 33.94º can be seen.

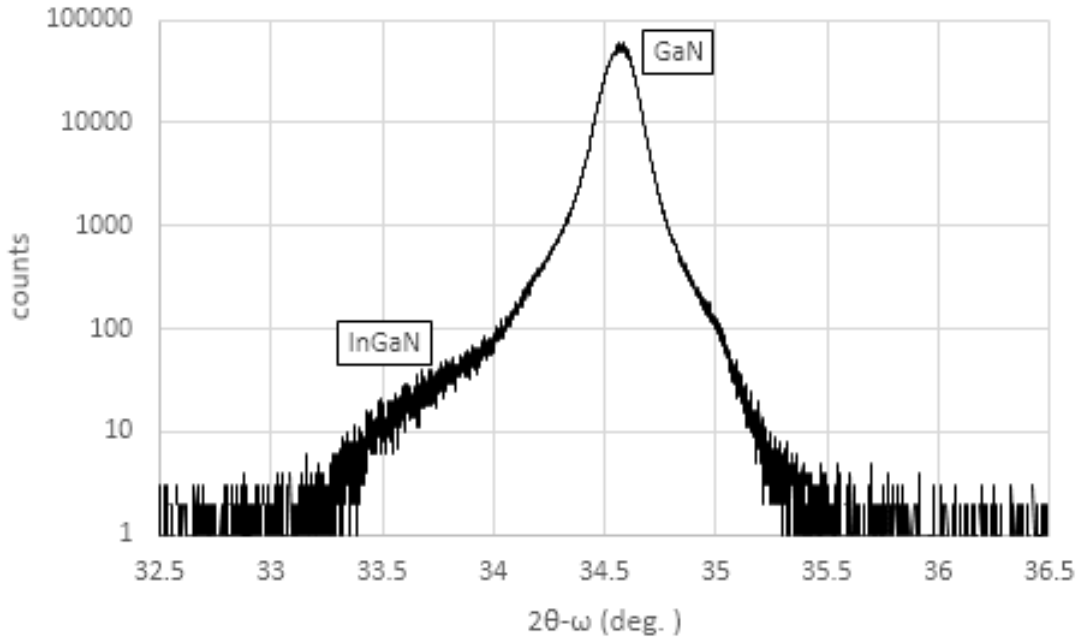

Figure 24: XRD plot of HP40 confirmed crystalline InGaN growth

4.2 Multiple Quantum Well Studies

4.2.1 Buffer Layer Investigation

4.2.1.1 Initial Buffer Layer Growths Results

Photoluminescence data was taken for the samples in the buffer layer experiment. Binary photoluminescence data can be seen in Table 8. In the data, it is immediately apparent that the only samples that produced significant PL had a high temperature GaN buffer layer. The low temperature GaN buffer layer, with a thicker film, produced a small amount of PL, but not on the same order as the samples with a high temperature buffer layer. The samples without a buffer layer did not produce any measurable PL, at room temperature. With the rest of the recipes being similar in nature, the buffer layer was the most significant difference between these growths, eliminating the need to examine multiple possibilities for the trend.

Table 8: Corresponding buffer layer and binary PL data

Sample	Buffer Layer	295°K PL	78°K PL
HP52	High Temp: 1100ºC$_{tc}$, 980ºC$_{substrate,\ estimated}$	Yes	Yes
HP53	High Temp: 1100ºC$_{tc}$, 980ºC$_{substrate,\ estimated}$	Yes	Yes
HP54	X	No	Yes
HP55	X	No	Yes
HP56	Low Temp: 930ºC$_{tc}$, 800ºC$_{substrate,\ estimated}$	Slight	N/A
HP57	High Temp: 1100ºC$_{tc}$, 980ºC$_{substrate,\ estimated}$	Yes	N/A

Because of this dependency of PL upon the buffer layer, an AFM investigation was done of sample HP54 and HP57, a sample with no buffer layer and one with a high temperature buffer layer, respectively. An AFM investigation was specifically chosen, because there was already some speculation on the quality of the nucleation and active layers, especially, in respect to the possibility that layers were being grown with InGaN islands, as opposed to indium incorporation across a complete 2D quantum layer.

The AFM scans were performed by another member of the group, John “Jack” Krause, and the data is show below, in Figure 25 a and b and Figure 26 a and b. In HP54, the one with no buffer layer, the growth appears to be pillar-esque; seemingly unconnected columns. The pillars, in the areas scanned, are from 10 to 50nm wide. The

height measurement of the tops of the pillars was between 40 and 49nm, while the bottom of the trench was between 15 and 25nm. The range of the measurements, between the tops of the pillars and the bottom of the trench, was between 20 and 34nm. This confirmed that the pillars were mostly unconnected, although some coalescence had begun, at their bases. This also indicates that the material did not initially coalesce, and grow as a 2-D, epitaxial layer, but rather, the growth continued upward, and probably sideways, creating pillars and islands that coalesced, at the bottom, as they grew.

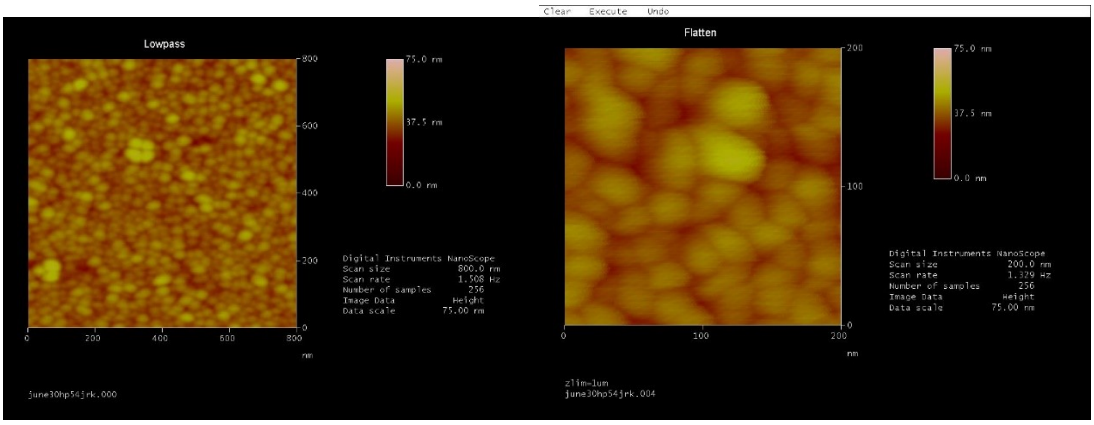

Figure 25: AFM of HP54, grown with no buffer layer, showing island growth

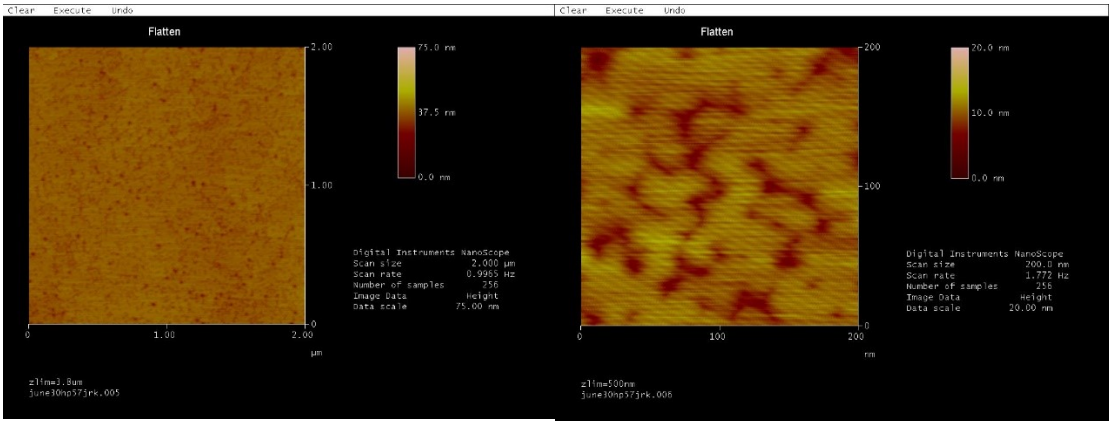

Figure 26: AFM of HP57, grown with a high temperature buffer layer, showing islands coalescing

In HP57, the one grown with a high temperature buffer layer, the growth no longer appears completely pillar-like, although there are still trenches in the growth. In HP57, many of the columns have coalesced, creating some continuous growth. The remaining trenches that have significantly less depth than sample 54, at approximately 6.5 - 10nm deep, instead of 20 - 34nm deep.

Nucleation was not expected to be a significant factor in these growths. This was largely due to the fact that these growths were all performed on GaN templates, making it homogenous, lattice-matched growth. However, it is evident that the nucleation/buffer layer is an important factor in the quality of the samples and that work needs to be done on the nucleation layers.

The photoluminescence and AFM data both point towards similar conclusions, about the buffer layer. The photoluminescence data shows that there is no room temperature PL for the samples that did not have a buffer layer, grown under the active layers. HP56, the sample that was grown with a low temperature buffer layer, showed minimal PL. However, the samples with high temperature buffer layers all had PL and had significantly increased PL intensities. The photoluminescence data alone, shows that the high temperature buffer layers are beneficial to the samples' luminescent properties.

The AFM data, from HP54 and HP57, adds understanding to the photoluminescence data. The processes seen, appears to be similar to the process of starting GaN growth on bare Al_2O_3, without the need to account for lattice-mismatch. The island growth, evident in the AFM scans, is seen in both samples. It looks like the growths are starting with separated nucleation sites, and the new material starts growing in island formations. In HP54, the island formations are prominent, with very little

continuity between tops. The trench measurements, with depths of 20- 34nm, show that some coalescence has happened at the lower layers of the approximately 56nm structure.

However, HP57, grown with a high temperature buffer layer, show significantly more coalescence of the material “islands”. The depth of the trenches, between the islands, is also reduced to 6-10nm, instead of 20-34nm. This shows that the islands have coalesced, but are still in a 3D growth pattern; not enough material has been grown to reach 2D growth.

The reason for the smoother surface, in HP57, is thought to be due to growth time and kinetics. The first reason is that growing a buffer layer simply gives the material islands more time to grow towards each other and connect, as seen in Figure 27. As the islands grow on all sides, they eventually meet. Once they have met, their crystal structures connect, possibly resolving with defects, as they begin to form a single, crystal lattice. Having the buffer layer grown first, means that the active layer(s) are grown on a flatter surface and are closer to an epitaxial growth mode.

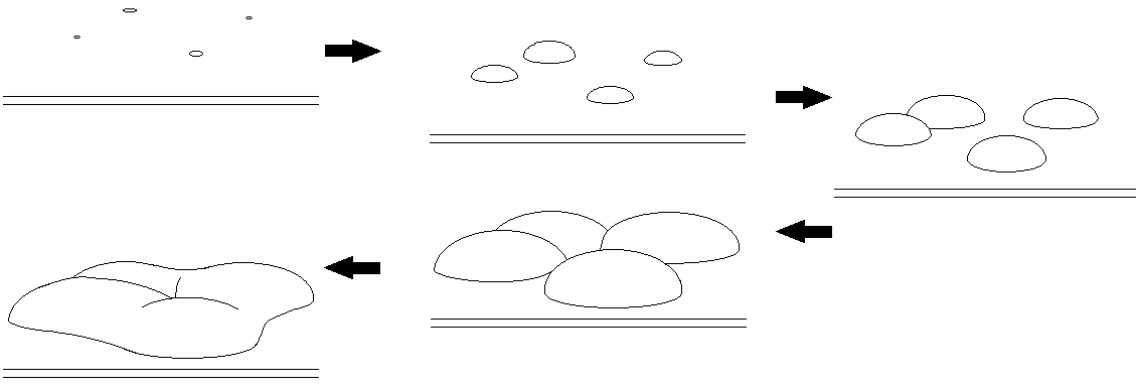

Figure 27: Illustration of nucleated islands, coalescing during growth

However, if this were the only mechanism at work, the low temperature buffer layer should have the same results as the high temperature buffer layer. The hypothesis proposed, is that the high temperature buffer layer also gives an added benefit, of higher quality GaN, and atoms that have a higher surface mobility. The increase in the surface mobility would give atoms the ability to move farther away from the islands where nucleation has started, allowing the columns to coalesce quicker. This would decrease the amount of total 3D growth, bringing the growth much closer to the desired 2D state before growing the active layers.

AFM of HP56, the sample with a low temperature buffer layer was not done. This would need to be completed, to compare with the surfaces of HP54 and HP57. This comparison would help verify the magnitude of the proposed effects. If the islands have coalesced, in a similar way as HP57, with the high temperature layer, the benefit is largely due to the increase in the quality of the layer. However, if the islands have made less progress towards 2D growth, the surface roughness is, most likely, having a large effect on the intensity of the photoluminescence.

4.2.1.2 Buffer Layer DOE Results

The two parameters were temperature and thickness. It had already been found, that ~980 which is 1100°C at the thermocouple, produced better results than the ~810°C, 930°C at the thermocouple, so the leading question was whether the temperature should be increased further. The secondary question was how a thin layer, approximately 4-6 nm compared to the approximately 25nm layers that were being grown.

Four samples were grown, two, referencing the thermocouple temperature, at 1200°C, and two at 1100°C. Two samples were grown at each temperature, one for each

layer thickness. The samples with buffer layers grown at 1200°C had no room temperature PL. An additional, thicker sample was grown at 1200°C, approximately 62nm thick, but it also produced no room temperature PL. Buffer layers grown at 1200°C seemed to be ruining the optical qualities of the sample. The problems caused by growth at 1200°C were not further investigated, as 1200°C is the upper range of the GaN process window, and most likely would have taken significant recipe changes to obtain a functional buffer layer at that temperature.

In the samples with buffer layers grown at 1100°C, the 25nm layer produced a sample that had 4.54 times the luminescent intensity of the 5nm buffer layer sample. This was attributed to the effect seen in the AFM scans of samples HP54 and HP57. The thinner buffer layer should have better coalescence than sample HP54, with no buffer layer, but would not have produced the amount of coalescence that was seen in sample HP57. The results of the PL DOE can be seen in Figure 28.

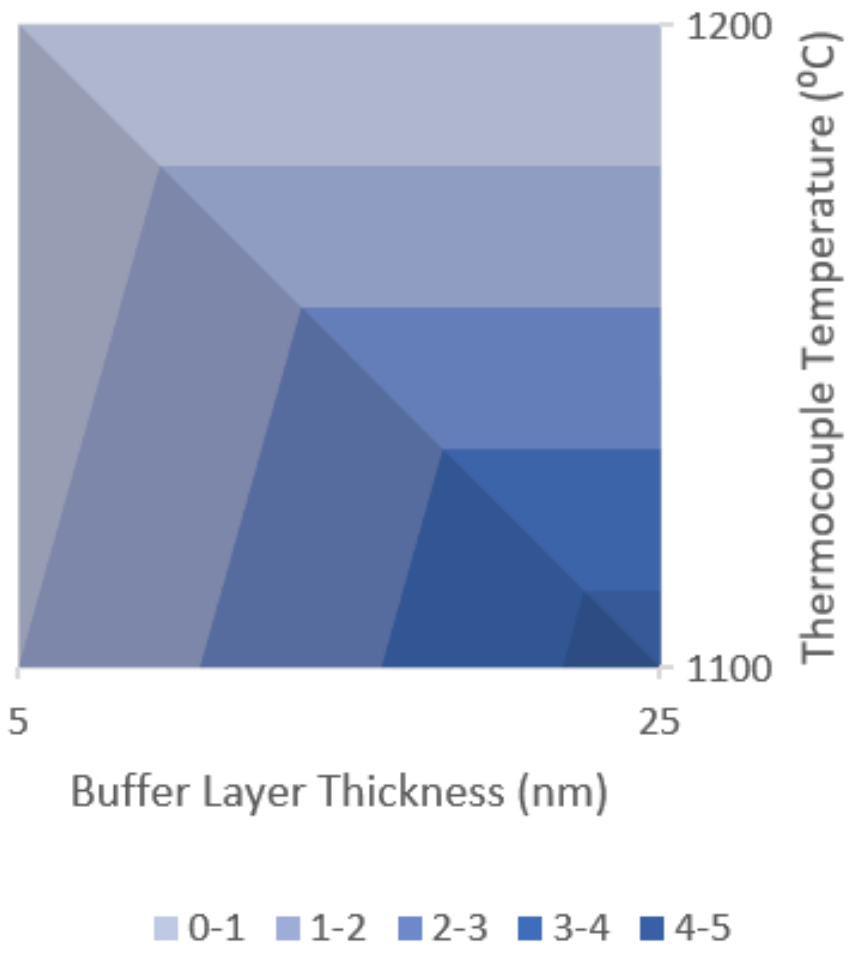

Figure 28: High temperature buffer layer DOE results showing PL intensity relative to the 5nm, 1100ºC sample, which was normalized to 1

The buffer layer DOE supported the conclusions of the first experiment. The DOE was designed to test whether a thin nucleation layer could produce the same results as the thicker nucleation layers, as well as give indicators on which way to adjust the buffer layer temperature and thickness. All of the buffer layers were high temperature layers. The DOE confirmed that the thicker buffer layers (25nm) performed better than the thinner buffer layers (5nm), which agrees with the conclusions of HP52- HP57. The PL results of HP57 were also repeated in the sample with the same high temperature buffer

layer, giving confidence in the repeatability of the experiments and accuracy of the conclusion.

One finding of the DOE is that there is an upper limit to the temperature of the buffer layer. On the temperature axis, of the DOE, 1100 and 1200C buffer layers were used. The 1200C buffer layers did not produce any room temperature PL. Although the reason is not completely known, this puts a temperature limit on the process used. Due to the resolution of this DOE, the actual upper limit is not known.

Filling out the DOE, with the only information we know, would indicate that the temperature of the buffer layer should be lowered. However, the expectation is that there is a curve, Gaussian or otherwise, with an optimal temperature at the center. Because one side of the DOE exceeded the current process temperature limit, localized curve data was not revealed.

4.2.2 Photoluminescence over Pressure Results

This experiment was done to see the effects of increasing the pressure in the reactor for growths. There are two theories that are expected to come into play here, the increased stabilization of the ternary alloy, as the MacChesney data indicates, and an increase in the IQE, as data from Dave Bour and Dr.Stokes indicates, should happen as the N partial pressure increases [13] [26]. For this experiment, a series of MQWs were grown, at increasing pressures. The respective volumetric flow of the group-V precursor was kept constant to obtain an increase in group-V partial pressure with the increase of total reactor pressure.

The group-III molar flow was kept constant throughout the experiment. Reductions in carrier gas flows through the bubblers and temperatures in the bubblers

was necessary to achieve this. By keeping the group-III molar flow constant and keeping the volumetric flow of the group-V precursor constant, the V:III ratio was increased as the pressure increased. This is the one extraneous change that was allowed during this experiment.

The increase in the V:III ratio was not expected to have a large impact on the outcome of the growths, although it could have some effect. Because there is adequate group-V precursors to participate in the reaction, and the experiment increases the V:III ratio, no effect from the perspective of inadequacies in the reaction is expected, as was seen in the first attempt to use known, low pressure processes. However, the increase in group-V atoms on the surface could affect the kinetics of the group-III atoms, most significantly by reducing their surface mobility [35]. This has been shown to change growth modes from island growth to step growth [8], but the samples should already be in step growth mode, even in the lowest V:III ratio employed in this experiment. The two other effects that could happen, is a widening of the FWHM, due to inhomogeneous composition, with respect to the group-III atoms, and an increase in the roughness of the sample's surface [41]. It has been shown that reducing the group-III mobility, through an increase in the V:III ratio, can lead to the inability of the group-III atoms to travel enough distance across the surface to achieve compositional equality across the sample. The growths and their parameters can be seen in Table 9.

Table 9: Pressure experiment samples and respective changed parameters

Sample	Pressure	P_{NH3}	V:III Ratio
HP76	1.5	0.55	90k
HP81	1.75	0.64	105k
HP78	2.0	0.73	120k
HP80	2.25	0.82	125k
HP79	2.5	0.91	150k

An unintended parameter was introduced into the experiment, due to the fact that instrument analysis happened after the growths were complete. This was a fluctuation in the difference in actual substrate temperature and measured substrate temperature. Referencing the previously mentioned design of the heater, susceptor, and thermocouple (Figure 6), the system is somewhat susceptible to undetected changes in substrate temperature. This can be caused by things like a slight height change in the susceptor at times of maintenance.

The method of calibrating the system is to take the system to the process window (thermocouple temperature, pressure), with only N_2 flowing. Then, with all light sources off, take an optical spectrum inside the reactor. This is done through the Filmetrics system that is used to monitor growth. The detector does not go deep into the IR, so only the high energy tail of the black body spectrum is obtained. Due to the way the reactor is designed, the black body curve is almost solely from the susceptor, and the heater is underneath the molybdenum susceptor. The partial black body spectrum is curve fitted, using the mathematical tool Origin. To accomplish this, the black body data, acquired

through the Filmetrics system, is put into Origin. The black body function is put into Origin and a best fit algorithm is run, to output the temperature that would best fit the data.

The data for different thermocouple temperatures and pressures are listed in Table 10. As can be seen, the growths at 1.5, 1.74, 2.0, and even 2.25 have relatively low variance in temperature, although the trend is downward with increases in pressure. However, there seems to be a significantly larger jump at 2.5 bar(a), making this growth temperature lower than the growth temperature at 1.5 bar(a) by 31°C. This is enough for measureable changes in process outcomes, although the expected effect would be a lower quality crystal, due to several effects. These include lower surface mobility of the atoms, a possible increase in group-III atoms on the surface, and a general reduction in structural quality. Since the binaries are expected to become more stable at higher pressures, an increase in the IQE and quality of the material is expected, without the temperature issue. If, upon characterization of the samples, an increase is still found, it should be despite the lower temperatures, not because of them. This means, if an increase in quality is found, it would have been even greater if the correct temperatures were used.

Table 10: Thermocouple and fitted temperatures at various pressures

$Temp_{Thermocpl}$ (°C)	Pressure (bar-a)	Fitted Temp (°C)	ΔT (°C)
930°C	1.5	870	60
	1.74	867	63
	2.0	863	67
	2.25	858	72
	2.5	839	91
	3.0	830	100
1100°C	1.5	1066	34
	2.0	1062	38
	2.5	1061	39

The samples in this experiment were mainly analyzed with photoluminescence at room temperature and at 77/78°K. Although this is not the true IQE, which can be accurately measured with liquid helium around 4-8°K, a liquid helium cryostat was not available for this work, so liquid nitrogen was used instead. The 77/78°K measurement gives an upper bound on the IQE and a good reference point for comparing the quality of the samples and will be called the IQE figure of merit. The samples, with their estimated growth temperatures can be seen in Table 11.

Table 11: Samples with corrected temperature data

Sample	Pressure	Temperature	V:III Ratio
HP76	1.5	870	90,000
HP78	2.0	863	120,000
HP79	2.5	839	150,744

Room temperature and 78K photoluminescence data was taken for the samples in this experiment. Data from the photoluminescence measurements can be seen in Table 12. As mentioned above, and IQE estimate, or upper bound was found, by dividing room temperature PL by 78K PL. This data can be seen in Table 13.

Table 12: Photoluminescence data for samples HP76, HP78, and HP79

Sample	Pressure (bar-a)	Intensity (295k)	λ (nm) (295k)	FWHM (nm, 295k)	Intensity (78k)	λ (nm) (78k)	FWHM (nm, 78k)
HP76	1.5	16.50	420	51.8	420	419	56.52
HP78	2.0	438.63	414.79	44.57	2520	407	56.54
HP79	2.5	345.97	410.86	29.83	1998	399.76	49.2

Table 13: 78ºK IQE estimate

	HP76	HP78	HP79
IQE Estimate (78K)	0.0003 (0.03 %)	0.174 (17.4%)	0.173 (17.3%)

It can be quickly seen that there are several trends versus pressure, even in the base data. For overall luminescent intensity, HP76, at 1.5 bar(a), had the lowest photoluminescent peak intensity, with a value only 2x the noise level of the measurement, in the current configuration. HP78, at 2.0 bar(a) had the greatest intensity, at room temperature and at low temperature. HP79, grown at 2.5 bar(a), had a slight decrease, when compared to HP78, but was much higher than HP76. HP79 was 79% of HP78's room and low temperature intensity measurements. However, it was 21 times the room temperature intensity of HP76 and 4.8 times the low temperature intensity of HP76. This data can be seen in a graph in Figure 29.

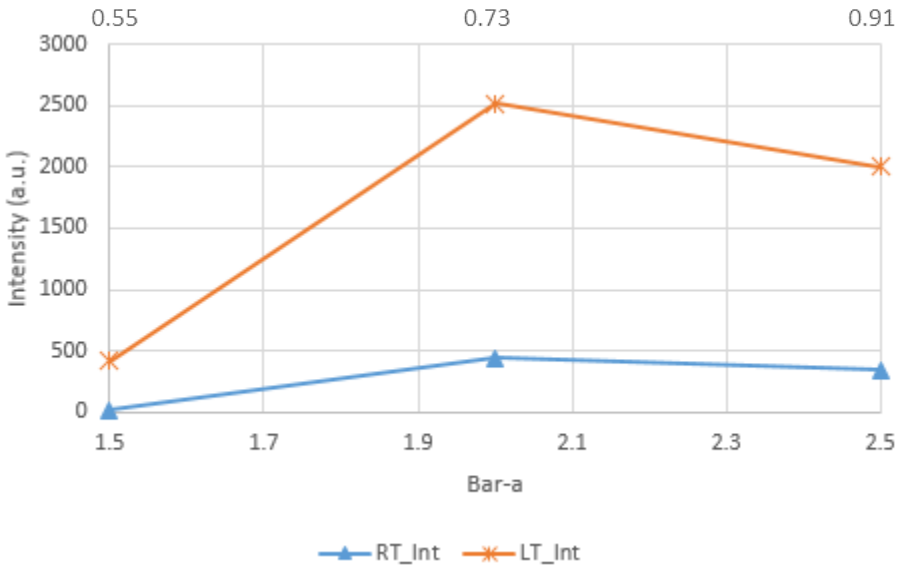

Figure 29: Luminescent intensity vs growth pressure/NH_3 partial pressure

This would lead to the observation that a pressure near 2.0 would be ideal for maximizing luminescent output, using this recipe. However, when taking the unintended substrate temperature decrease into account versus the amount of decrease between the

intensity at 2.0 bar(a) and 2.5 bar(a), it is likely that the 2.5 bar(a) growth would have an increased luminescent output when grown at the same temperature as the 2.0 bar(a) growth. This hypothesis is based upon other experiments within this work that have all confirmed that increasing the growth temperature increases the luminescent intensity, up to a suspected limit which was not reached in this work.

The center wavelength of the InGaN emitter changed with pressure also. As the pressure increased, the center wavelength blue-shifted, as seen in Figure 30. This most likely corresponds to a decrease in indium content within the InGaN semiconductor and is counter to the effect that decreasing temperature would have. Decreasing the temperature would increase the amount of indium by reducing the rate of indium desorption and decreasing the thermal energy available to break the In-N bonds in the lattice [25]. The current growth temperature is shown to be above the stable temperature for the InN binary, although the author is unaware of any work determining formula and definitive relationships for the thermodynamic stability regions of the ternary InGaN.

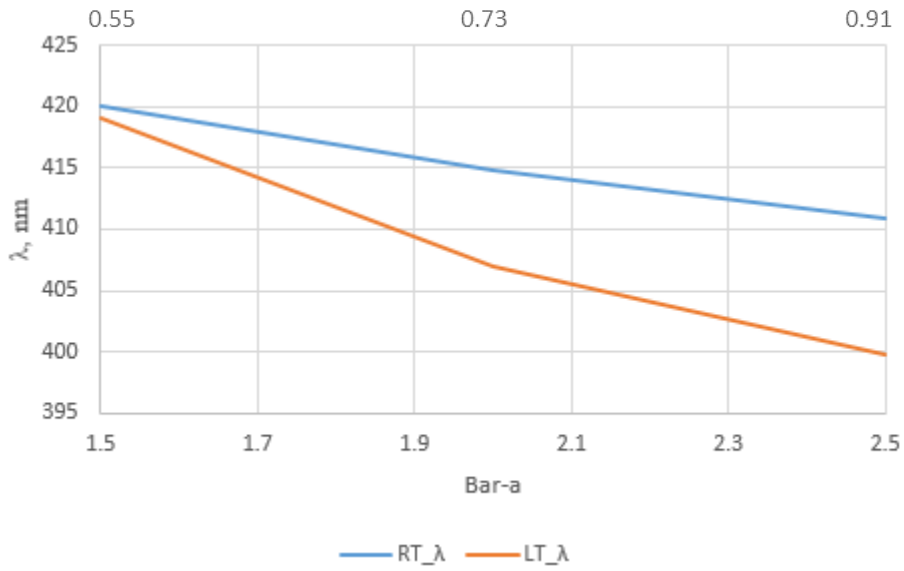

Figure 30: InGaN emission peak, blue shifting with increased pressure

Because the effect is counter to the effect of the temperature variance in the growth, this effect should be due to the pressure increase, which can be interpreted as an increase in the group-V partial pressure [26]. This observation is supported by work from Dong-Joon Kim, et. al., who acknowledges the possibility that the decreased growth rate that came with the increase in pressure could be responsible for this [24]. A decrease in growth rate with increase in pressure has been observed during this work as well. To completely confirm that this is indeed the case, a secondary measurement, such as XRD would need to be performed and the data correlated.

Finally, the FWHM of the peaks changed significantly with pressure. The FWHM at low temperature stayed somewhat stable, with no more than a 13% decrease between 1.5 and 2.5 bar(a), as seen in Figure 31. However, the FWHM of the room temperature peaks changed significantly with pressure, decreasing by 58%. The data can be seen in

Figure 31 as well. It is interesting to note that the change in FWHM (78k FWHM – 295k FWHM) is approximately linear vs pressure or NH_3 partial pressure.

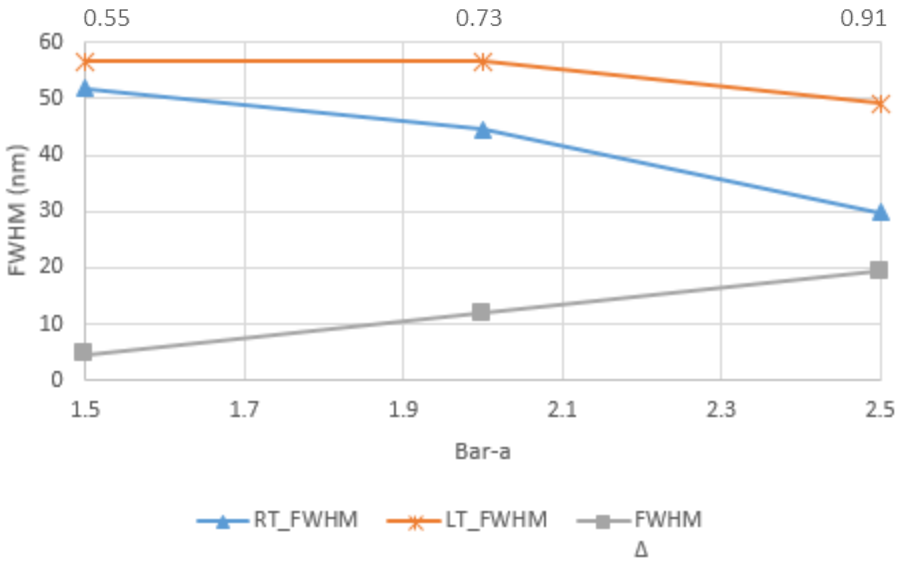

Figure 31: FWHM and FWHM Δ vs pressure

This data indicates a decrease in deviation in InGaN composition with pressure. As with the luminescent intensity, this contradicts what would be expected, if it were correlated with the unintended decrease in temperature, leaving the effect to be due to the pressure increase. The hypothesis, which would have to have XRD data to completely back it up, is that the increase in pressure caused greater compositional control within the sample. Because the increase in pressure cause, directly or indirectly, lessened the indium content within the samples, the narrowing of the FWHM with pressure could be partially due to the lessened strain on lattice allowing higher quality growth.

Taking the photoluminescence data, the IQE figure of merit was calculated for the three samples. The data can be seen in Figure 32. There was an initial increase between

HP76 and HP78. However, there was a slight decrease between HP78 and HP79, but they were within 0.52% of each other. Because the temperature decrease is thought to have affected the luminescent intensity, which is supported by other experiments within this work, there is a high likelihood that the IQE FOM was directly influenced as well. An increase in temperature "generally" produces higher quality InGaN, inside certain process limits. There are several factors that influence this, one of them is that the increase in thermal energy assists in completing pyrolysis of the precursors, which decreases impurity defects in the semiconductor. The increase in energy also increases the ability of the atoms to reach their proper lattice sites before additional layers are grown.

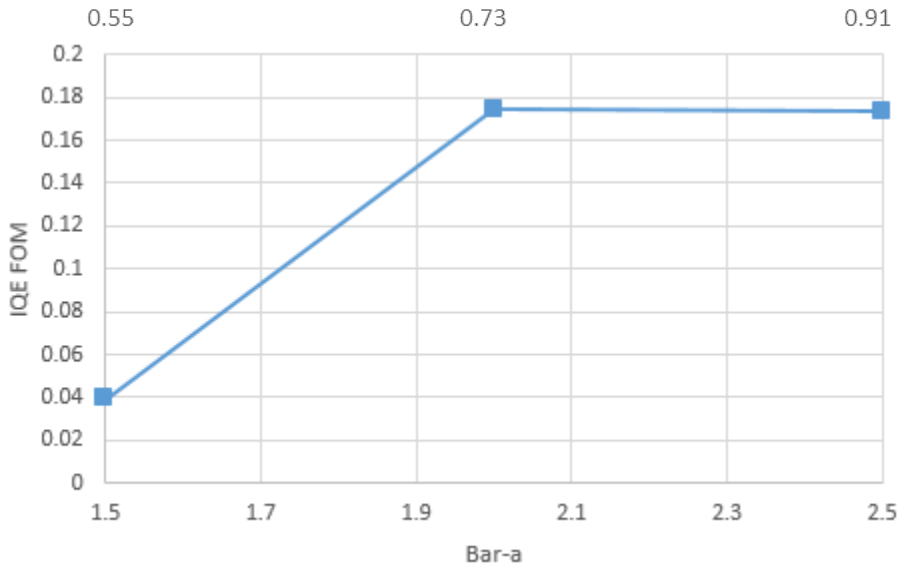

Figure 32: IQE figure of merit vs pressure

However, the indium composition of the InGaN was decreased as pressure increased, which leaves less strain on the layer. This is most likely contributing to a lessened defect density in the crystal and a higher IQE FOM, along with the increase in

NH_3 partial pressure, which should be decreasing N-vacancy defects, a known non-radiative recombination center.

CHAPTER 5: CONCLUSIONS

5.1 InGaN Thin Film Studies

5.1.1 Group-III Flux Investigation Conclusions

The first growth showed signs of excess indium metal deposition and little to no signs of crystal growth. However, this was where the development of super-atmospheric MOCVD processes, with the custom, CFD-designed reactor began. The next two growths successfully decreased the amount of indium deposition. An increase in growth temperature, from ~630ºC to 750ºC, caused a 37.8% decrease in indium content on the sample (-0.315%In / ºC). No representation is made on the linearity in this region. This shows a strong dependence, of indium stability, upon temperature alone.

In the second stage of the experiment, the total indium flow was reduced by 75% and the sample thickness was reduced by 44%. It was shown that these changes had a near 1:1 (1.075:1) reduction in the excess indium content on the sample. The main discrepancy is expected to be related to the fact that when the In precursor flow was reduced, the In:Ga ratio was held constant. This means the Ga precursor flow was reduced to 25% of its previous flow as well. This could account for part of the In content not changing in a 1:1 fashion.

This experiment established a limit on this particular process. With growth temperature of ~750ºC, at 1.5 bar(a), and a V/III ratio of ~30,000, the group-III flux needs to be in the range of 15µmol/min or less.

5.1.1.1 Follow Up Experiment: Lower In:Ga Ratio, Higher Temperature Conclusions

This experiment, following the prediction of the previous experiment, showed that InGaN could be grown with superatmospheric processes. It also demonstrated that the high In:Ga ratios reported in many low pressure processes, are not necessary, with these recipes. This shows an increase in the stability of the indium in the growth process.

This experiment also showed that the current growth process, at the time of this experiment, produced group-III/group-V and carbon content in line with industry-grown GaN templates. This is a significant conclusion to the group-III flux experimental thrust.

5.1.2 Photoluminescence and Growth Temperature Conclusions

Growing a set of samples over common growth temperatures demonstrated that an increase in temperature increases the intensity of the photoluminescence. From this work, this can only be said for the range of processes that were worked with, ~700ºC to 800ºC. It was also shown that the PL intensity vs temperature function is not linear, but it was not demonstrated why. Little to no dependence of the indium concentration (as estimated by PL peak) was seen between the temperature ranges investigated, which is also significantly different from low pressure growths, at these temperatures.

5.2 Multiple Quantum Well Studies

5.2.1 Buffer Layer Investigation

5.2.1.1 Initial Buffer Layer Growths Conclusions

Nucleation was not initially expected to play a large role in these growths, due to the GaN templates that were being used. This experiment showed that the nucleation/buffer layer played a significant role in the structure and optical quality of the InGaN that was grown. Higher temperature buffer layers (1100ºC at the thermocouple)

performed significantly better than buffer layers grown at the InGaN growth temperatures. Samples that were grown with no buffer layer did not produce any room temperature photoluminescence.

5.2.1.2 Buffer Layer DOE Conclusions

The buffer layer DOE revealed several points of interest. It showed that a thin buffer layer did not produce the same results as a thicker one (5nm vs 25nm). This was originally being investigated, since the need for a buffer layer was now established, the remaining question was whether or not a process, like the thin buffer layers on Al_2O_3, would be a sufficient solution. The DOE indicated that thicker is better, but it was not continued to find the point of diminishing returns.

An interesting and unexpected point was found. Buffer layers, grown at a thermocouple temperature of 1200ºC, seemed to be as destructive to the sample's optical qualities as no buffer layer. Although the reasoning behind this was not fully investigated, an upper limit was put on the buffer layer processes.

5.2.2 Photoluminescence over Pressure Conclusions

This experiment resulted in several findings. The first is that photoluminescent intensity increased from 1.5 bar(a) to 2.0 bar(a) and had a relatively small decrease between 2.0 bar(a) and 2.5 bar(a). However, there was an unintended decrease in growth temperature between 2.0 bar(a) and 2.5 bar(a) of 24ºC. Since it is well established that growth temperatures, within their limits, increase crystal quality, and therefore associated luminescent intensity, it is possible that the unintended decrease in temperature has decreased the photoluminescent intensity of the 2.5 bar(a) sample. If true, this would put the 2.5 bar(a) growth at a similar or higher intensity than the 2.0 bar(a) growth. With the

decrease in temperature only being 7ºC between 1.5 bar(a) and 2.0 bar(a), it is definitively shown that the increase in growth and NH_3 pressures increased photoluminescent intensity.

The IQE FOM also increased, then stabilized, as the pressure increased. This is the IQE FOM, estimated by photoluminescence at 295K and 78K. Similar to the photoluminescent intensity measurement, it showed a significant increase from 1.5 bar(a) to 2.0 bar(a), but was mostly stable from 2.0 bar(a) to 2.5 bar(a). There was a minimal decrease between 2.0 bar(a) and 2.5 bar(a), but this was within the noise of the measurement. The decrease in temperature between 2.0 bar(a) and 2.5 bar(a) is thought to have affected this in the same way.

The FWHM of the photoluminescence peaks decreased with pressure. Since a decrease in temperature would have the opposite effect, the dominant process parameter affecting this is attributed to pressure. This indicates that the InGaN active layers' homogeneity has increased with pressure. However, there was a blue shift in the photoluminescence spectrums, with pressure. Having less indium, in the crystal, would have reduced strain and could be assisting in the FWHM measurements.

The improvement in optical quality, especially between 1.5 bar(a) and 2.0 bar(a) can be attributed to multiple things. One of the theories that started the work with the HP-MOCVD, was that there is a curve, similar to the III-Arsenides and III-Phosphides, relating luminescent intensity to group-V partial pressures, as seen in Figure 8. One of the attributes of this is that V-pitting and N deficiencies (non-luminescing defects) would be decreased with increasing group-V partial pressure. While this work did not prove that this is indeed the mechanism at work, the data is in agreement with that theory. [42]

CHAPTER 6: RECOMMENDATIONS

If this work is continued, it is highly recommended that research on the active layer(s) itself is temporarily paused, and work on the nucleation and buffer layers is continued. This work showed the effect that the nucleation/buffer layer has on samples that are grown on lattice-matched, native substrate (GaN on Al_2O_3). To continue this work, it would be prudent to take AFM scans of HP56 and investigate HP56 vs. HP57. This comparison would help verify the magnitude of the proposed effects. If the islands have coalesced, in a similar way as HP57, with the high temperature layer, the benefit is largely due to the increase in the quality of the layer. However, if the islands have made less progress towards 2D growth, the surface roughness is, most likely, having a large effect on the intensity of the photoluminescence.

The answer to this would direct future work on the buffer layer. It would dictate whether to start on the quality of the GaN, or the effects of achieving 2D growth, before starting the growth of the active layers. Both should probably need investigation.

Because the DOE found an upper limit on the buffer layer growth process, a DOE, with tighter limits should be conducted. It is recommended that the same two variables are used, but use tighter temperature changes. For example, use 1075 and 1125, instead of 1100 and 1200C. Because the thicker buffer layer performed better, it is recommended that the investigation would continue and use even thicker buffer layers. It would be expected that the local PL intensity slope of 0.1375/nm, would not continue

indefinitely. It may increase before decreasing, but diminishing returns would be expected, as 2D growth is reached, and the island's lattices connect.

Preliminary work was started with the V:III ratio. The first sample (HP77), although not explicitly mentioned in this work, shows indication that a lowered V:III ratio (12,000) produces a more intense and more defined InGaN peak, during XRD. This is possibly due to improvements in surface roughness and/or structure. However, sample HP77 did not have the highest PL intensities of the samples worked with. It is recommended that future work investigates the area of optimal V:III ratios further. It is especially recommended that low V:III ratios, combined with high NH_3 partial pressures are investigated.

Additionally, the latter part of this work moved towards using multiple quantum wells. This was done, to increase the intensity of the PL and make optical characterization easier. However, it made XRD characterization significantly harder, as well as diminished the relevance of X-Ray fluorescence measurements. It also added extra variability factors to the experiments, which is not desirable, at this point in the research. It is highly recommended that the research goes back to using InGaN films, unless it is necessary for specific optical characterizations.

REFERENCES

[1] Goetz, Werner; LUMILEDS, "LED Science and Technology Advancements," in *DOE SSL R&D Workshop*, Nashville, TN, 2018.

[2] A. G. Melton, P. Davis, M. Uddin and E. B. Stokes, "Superatmospheric MOCVD Reactor Design For High Quality InGaN Growth," *ECS Transactions,* vol. 45, no. 7, pp. 73-77, 2016.

[3] O. Ambacher, "Growth and applications of Group III-nitrides," *Journal of Physics D: Applied Physics,* vol. 31, pp. 2653-2710, 1998.

[4] J. Wu, W. Walukiewicz, K. M. Yu, J. W. Ager III, E. E. Haller, H. Lu, W. J. Schaff, Y. Saito and Y. Nanishi, "Unusual properties of the fundamental band gap of InN," *Applied Physics Letters,* vol. 80, p. 3967, 2002.

[5] W. Jiang, D. Ehrentraut, B. C. Downey, D. S. Kamber, R. T. Pakalapati, H. D. Yoo and M. P. D'Evelyn, "Highly transparent ammonothermal bulk GaN substrates," *Journal of Crystal Growth,* vol. 403, pp. 18-21, 2014.

[6] I.-h. Ho and G. B. Stringfellow, "Solid phase immiscibility in GaInN," *Applied Physics Letters,* vol. 69, no. 18, pp. 2701-2703, 1996.

[7] G. T. Thaler, D. D. Koleske, S. R. Lee, K. H. A. Bogart and M. H. Crawford, "Thermal stability of thin InGaN films on GaN," *Journal of Crystal Growth,* vol. 312, pp. 1817-1822, 2010.

[8] F. K. Yam and Z. Hassan, "InGaN: An overview of the growth kinetics, physical properties and emission mechanisms," *Superlattices and Microstructures,* vol. 43, pp. 1-23, 2008.

[9] Z. Dridi, B. Bouhafs and P. Ruterana, "First-principles investigation of lattice constants and bowing parameters in wurtzite AlxGa1-xN, InxGa1-xN and InxAl1-xN alloys," *Semiconductor Science and Technology,* vol. 18, pp. 850-856, 2003.

[10] D. Queren, M. Schillgalies, A. Avramescu, G. Bruderl and A. Laubsch, "Quality and thermal stability of thin InGaN films," *Journal of Crystal Growth,* vol. 311, pp. 2933-2936, 2009.

[11] A. H. White and W. Melville, "The decomposition of ammonia at hight temperatures," *Journal of the American Chemical Society,* vol. 27, no. 4, pp. 73-386, 1905.

[12] A. C. Jones, S. A. Rushworth, J. R. Brown and D. J. Houlton, "Alterative Precursor Systems for the MOCVD of Aluminium Nitride and Gallium Nitride," *Advanced Materials for Optic and Electronics,* vol. 6, pp. 119-126, 1996.

[13] J. B. MacChesney, P. M. Bridenbaugh and P. B. O'Connor, "Thermal Stability of Indium Nitride at Elevated Temperatures and Nitrogen Temperatures," *Material Research Bulletin,* vol. 5, pp. 783-792, 1970.

[14] Z. Ma, H. Yang, H. Wu, W. Hu, Y. Jiang, W. Wang, H. Jia, J. Zhou and H. Chen, "Alleviation of parasitic reactions for III-nitride epitaxy in MOCVD with a spatially separated source delivery method by controlling the main reaction type," *Journal of Crystal Growth,* vol. 465, pp. 1-5, 2017.

[15] A. C. Jones, C. R. Whitehouse and J. S. Roberts, "Chemical Approaches to the Metalorganic CVD of Group-III Nitrides," *Chemical Vapor Deposition,* vol. 1, no. 3, pp. 65-74, 1995.

[16] R. Togashi, T. Kamoshita, Y. Nishizawa, H. Murakami, Y. Kumagai and A. Koukitu, "Experimental and ab-initio studies of temperature dependent InN decomposition in various ambient," *Physica Status Solidi C,* vol. 5, no. 6, pp. 1518-1521, 2008.

[17] S. Keller, B. P. Keller, D. Kapolnek, U. K. Mishra, S. P. DenBaars, I. K. Shmagin, R. M. Kolbas and S. Krishnankutty, "Growth of bulk InGaN films and quantum wells by atmospheric pressure metalorganic chemical vapour deposition," *Journal of Crystal Growth,* vol. 170, pp. 349-352, 1997.

[18] T. Matsuoka, N. Yoshimoto, T. Sasaki and A. Katsui, "Wide-Gap Semiconductor InGaN and InGaAlN Grown by MOVPE," *Journal of Electronic Materials,* vol. 21, no. 2, pp. 157-163, 1992.

[19] N. Yoshimoto, T. Matsuoka, T. Sasaki and A. Katsui, "Photoluminescence of InGaN films grown at high temperature by metalorganic vapor phase epitaxy," *Applied Physics Letters,* vol. 59, no. 18, pp. 2251-2253, 1991.

[20] N. Dietz, M. Alevli, V. Woods, M. Strassburg, H. Kang and I. T. Ferguson, "The Characterization of InN Growth Under High-Pressure CVD Conditions," *Physica Status Solidi b,* vol. 242, no. 15, pp. 2985-2994, 2005.

[21] Y. Huang, A. Melton, B. Jampana, M. Jamil, J.-H. Ryou, R. D. Dupuis and I. T. Ferguson, "Growth and characterization of InxGa1-xN alloys by metalorganic chemical vapor deposition for solar cell applications," *Journal of Photonics for Energy,* vol. 2, p. 028501, 2012.

[22] S. Nakamura, T. Mukai and M. Senoh, "High-Power P-N Junction Blue-Light-Emitting Diodes," *Japanese Journal of Applied Physics,* vol. 30, no. 12A, pp. 1998-2001, 1991.

[23] W. V. Lundin, E. E. Zavarin, M. A. Sinitsyn, A. V. Sakharov, S. O. Usov, A. E. Nikolev, D. V. Davydov, N. A. Cherkashin and A. F. Tsatsulnikov, "Effect of Pressure in the Growth Reactor on the Properties of the Active Region in the InGaN/GaN Light-Emitting Diodes," *Semiconductors,* vol. 44, no. 1, pp. 123-126, 2010.

[24] D.-J. Kim, Y.-T. Moon, K.-M. Song, I.-H. Lee and S.-J. Park, "Effect of Growth Pressure on Indium Incorporation During the Growth of InGaN by MOCVD," *Journal of Electronics Materials,* vol. 30, no. 2, pp. 99-102, 2001.

[25] Y. Kangawa, T. Akiyama, T. Ito, K. Shiraishi and T. Nakayama, "Surface Stability and Growth Kinetics of Compound Semiconductors: An Ab Iinitio-Based Approach," *Materials,* vol. 6, pp. 3309-3360, 2013.

[26] E. Stokes and D. Bour, "UNCC MRI Project Description," Unpublished, Charlotte, NC, 2008.

[27] H. Hahn and R. Juza, "Untersuchungen u"ber die Nitride von Cadmium, Gallium, Indium und Germanium. Metallamide und Metallnitride.," *Zeitschrift fu"r anorganische und allgemeine Chemie,* vol. 244, no. 2, pp. 111-124, 1940.

[28] S. Nakamura, Y. Harada and M. Seno, "Novel metalorganic chemical vapor deposition system for GaN growth," *Applied Physics Letters,* vol. 58, no. 18, pp. 2021-2023, 1991.

[29] S. Nakamura and T. Mukai, "High-Quality InGaN Films Grown on GaN Films," *Japanese Journal of Applied Physics,* vol. 31 Pt. 2, no. 10B, pp. 1457-1459, 1992.

[30] V. Woods and N. Dietz, "InN growth by high-pressures chamical vapor deposition: Real-time optical growth characterization," *Materials Science & Engineering B,* vol. 127, pp. 239-250, 2006.

[31] N. Dietz, "High-pressure CVD growth of InN and indium-rich group III-nitride compound cemiconductors for novel mid- and far-infrared detectors and emitters," Georgia State University, Department of Physics and Astronomy, Atlanta, Georgia, 2012.

[32] S. Nakamura, M. Senoh and T. Mukai, "Highpower InGaN/GaN doubleheterostructure violet light emitting diodes," *Applied Physics Letters,* vol. 62, no. 19, pp. 2390-2392, 1993.

[33] Y. Ohba, M. Ishikawa, H. Sugawara, M. Yamamoto and T. Nakanisi, "Growth of High-Quality InGaAlP Epilayers by MOCVD Using Methyl Metalorganics and their Applications to Visible Semiconductor Lasers," *Journal of Crystal Growth,* vol. 77, pp. 374-379, 1986.

[34] T. Takeuchi, Y.-L. Chang, A. Tandon, D. Bour, S. Corzine, R. Twist, M. Tan and H.-C. Luan, "Low Threshold 1.2um InGaAs Quantum Well Lasers Grown Under Low As/III Ratio," *Applied Physics Letters,* vol. 80, pp. 2445 - 2447, 2002.

[35] R. A. Oliver, M. J. Kappers, C. J. Humphreys and G. A. D. Briggs, "THe influence of ammonia on the growth mode in InGaN/GaN heteroepitaxy," *Journal of Crystal Growth,* vol. 272, pp. 393-399, 2004.

[36] T. Matsuoka, H. Tanaka, T. Sasaki and A. Katsui, "Wide-gap semiconductor (In,Ga)N," in *Int. Symposium GaAs and Related Compounds, Inst. of Phys. Conf. Ser.*, 1989.

[37] M. Leyer, J. Stellmach, C. Meissner, M. Pristovsek and M. Kneissl, "The critical thickness of InGaN on (0 0 0 1)GaN," *Journal of Crystal Growth,* vol. 310, pp. 4913-4915, 2008.

[38] S. M. Bedair, F. G. McIntosh, J. C. Roberts, E. L. Piner, K. S. Boutros and N. A. El-Masry, "Growth and characterization of In-based nitride compounds," *Journal of Crystal Growth,* vol. 178, pp. 32-44, 1997.

[39] C. G. Van de Walle, M. D. McCluskey, C. P. Master, L. T. Romano and N. M. Johnson, "Large and composition-dependent band gap bowing in InxGa1-xN alloys," *Materials Science and Engineering,* vol. B59, pp. 274-278, 1999.

[40] E. Hahn, A. Rosenauer, D. Gerthsen, J. Off, F. Scholz, M. Vehse and J. Gutowski, "Influence of growth kinetics on the indium distribution during MOVPE growth of GaInN quantum wells," *Physica Status Solidi C,* vol. 0, no. 7, pp. 2171-2176, 2003.

[41] R. Atalay, M. Buegler, S. Gamage, M. K. I. Senevirathna, B. r. Kucukgok, A. G. Melton, A. Hoffman, A. G. U. Perera, I. T. Ferguson and N. Dietz, "Effect of V/III molar ratio on the structural and optical properties of InN epilayers," in *Twelfth International Conference on Solid State Lighting and Fourth International Conference on White LEDs and Solid State Lighting, Proceedings of SPIE*, 2012.

[42] M. Conway, P. C. Deguzman and E. B. Stokes, "Superatmospheric MOCVD Growth of Bulk InGaN for Template and Optoelectronic Applications," *ECS Transactions,* vol. 61, no. 4, pp. 235-241, 2014.

[43] D. Ehrentraut, E. Meissner and M. Bockowski, Technology of Gallium Nitride Crystal Growth, New York, New York: Springer, 2010.

[44] M. Buegler, S. Gamage, R. Atalay, J. Wang, I. Senevirathna, R. Kirste, T. Xu, M. Jamil, I. Ferguson, J. Tweedie, R. Collazo, A. Hoffman, Z. Sitar and N. Dietz, "Reactor pressure - growth temperature relations for InN epilayers grown by high-pressure CVD," in *Tenth International Conference on Solid State Lighting, Proceedings of SPIE*, 2010.

[45] M. Buegler, S. Gamage, R. Atalay, J. Wang, M. K. I. Senevirathna, R. Kirste, T. Xu, M. Jamil, I. Ferguson, J. Tweedie, R. Collazo, A. Hoffman, Z. Sitar and N. Dietz, "Growth temperature and growth rate dependency on reactor pressure for InN epilayers grown by HPCVD," *Physica Status Solidi C,* pp. 2059-2062, 2011.

[46] G. Durkaya, M. Buegler, R. Atalay, I. Senevirathna, M. Alevli, O. Hitzemann, M. Kaiser, R. Kirste, A. Hoffman and N. Dietz, "The influence of the group V/III molar precursor ratio on the structural properties of InGaN layers grown by HPCVD," *Physica Status Solidi A,* vol. 207, no. 6, pp. 1379-1382, 2010.

[47] J. M. Wang, "Optical Properties of In 1-xGaxN Epilayers Grown by HPCVD," Physics and Astronomy Theses, Atlanta, Georgia, 2010.

[48] T. Nagatomo, T. Kuboyama, H. Minamino and O. Omoto, "Properties of Ga1-xInxN Films Prepared by MOVPE," *Japanese Journal of Applied Physics,* vol. 28, no. 8, pp. 1334-1336, 1989.

[49] A. Wakahara, T. Tokuda, X.-Z. Dang, S. Noda and A. Sasaki, "Compositional inhomogeneity and immiscibility of a GaInN ternary alloy," *Applied Physics Letters,* vol. 71, no. 7, pp. 906-908, 1997.

[50] D. D. Koleske, A. E. Wickenden, R. L. Henry, M. E. Twigg, J. C. Culbertson and R. J. Gorman, "Enhanced GaN decomposition in H2 near atmospheric pressures," *Applied Physics Letters,* vol. 73, no. 14, pp. 2018-2020, 1998.

[51] V. G. Deibuk and A. V. Voznyi, "Thermodynamic Stability and Redistribution of Charges in Ternary AlGaN, InGaN, and InAlN Alloys," *Semiconductors,* vol. 39, no. 6, pp. 623-628, 2005.

[52] Y. Huang, H. Wang, Q. Sun, J. Chen, J. F. Wang, Y. T. Wang and H. Yang, "Study on the thermal stability of InN by in-situ laser reflectance system," *Journal of Crystal Growth,* vol. 281, pp. 310-317, 2005.

[53] W. Fathallah, T. Boufaden and B. El Jani, "Analysis of GaN decomposition in an atmospheric MOVPE vertical reactor," *Pysica Status Solidi C,* vol. 4, no. 1, pp. 145-149, 2007.

[54] A. Bchetnia, I. Kemis, A. Toure, W. Fathallah, T. Boufaden and B. El Jani, "GaN thernal decomposition in N2 AP-MOCVD environment," *Semiconductor Science Technology,* vol. 23, pp. 1-5, 2008.

[55] T. Hikosaka, T. Shioda, Y. Harada, K. Tachibana, N. Sugiyama and S.-y. Nunoue, "Impact of InGaN growth conditions on structural stability under high temperature process in InGaN/GaN multiple quantum wells," *Physica Status Solidi C,* vol. 8, no. 7-8, pp. 2016-2018, 2011.

[56] K.-H. Lee, S. H. Park, J. H. Kim, N. H. Kim, M. H. Kim, H. Na and E. Yoon, "MOCVD growth of GaN layer on InN interlayer and relaxation of residual strain," *Thin Solid Films,* vol. 518, pp. 6365-6368, 2010.

[57] W. Lee, M.-H. Kim, D. Zhu, A. N. Noemaun, J. K. Kim and E. F. Schubert, "Growth and characteristics of GaInN/GaInN multiple quantum well light-emitting diodes," *Journal of Applied Physics,* vol. 107, 2010.

[58] D. Iida, K. Nagata, T. Makino, M. Iwaya, S. Kamiyama, H. Amano, I. Akasaki, A. Bandoh and T. Udagawa, "Growth of GaInN by Raised-Pressure Metalorganic Vapor Phase Epitaxy," *Applied Physics Express,* vol. 3, 2010.

[59] J. J. Coleman, "Metalorganic Chemical Vapor Deposition for Optoelectronic Devices," in *Proceedings of the IEEE*, 1997.

[60] X. Li, D. V. Forbes, S. Q. Gu, D. A. Turbull, S. G. Bishop and J. J. Coleman, "A New Buffer Layer for MOCVD Growth of GaN on Sapphire," *Journal of Electronic Materials,* vol. 24, no. 11, pp. 1711-1714, 1995.

[61] F. M. Morales, D. Gonzalez, J. G. Lozano, R. Garcia, S. Hauguth-Frank, V. Lebedev, V. Cimalla and O. Ambacher, "Determination of the composition of InxGa1-xN from straing measurements," *Acta Materiala,* vol. 57, pp. 5681-5692, 2009.

[62] D. Holec, P. M. F. J. Costa, M. J. Kappers and C. J. Humphreys, "Critical thickness calculations for InGaN/GaN," *Journal of Crystal Growth,* vol. 303, pp. 314-317, 2007.

[63] Y. Ohba, M. Ishikawa, H. Sugawara and T. Nakanisi, "Growth of high-quality InGaAlP epilayers by MOCVD using methyl organics and their application to visible semiconductor lasers," *Journal of Crystal Growth,* vol. 77, no. 1-3, pp. 374-379, 1986.

[64] T. Takeuchi, C. Y.-L. A. Tandon, D. Bour, S. Corzine, R. Twist and M. Tan, "Low threshold 1.2 micron InGaAs quantum well lasers grown under low As/III ratio," *Applied Physics Letters,* vol. 80, no. 14, pp. 2445-2447, 2002.

APPENDIX A: HIGH PRESSURE MOCVD STANDARD OPERATING PROCEDURES

Wafer/Substrate Loading

- Ensure that all systems are off or disconnected from the reaction chamber. Ex: vacuum pump, gas flows, susceptor motor
- Remove reaction chamber lid and set it on the white block, being careful not to put tension on the fiber optics cable or analog pressure transducer line. If bolted down, remove bolts, putting them in the small, yellow bin labeled curve to can. If gas lines are connected, use wrench to disconnect line and discard used gasket.
- Using wafer tweezers, put 2" wafer/substrate in the routed pocket, matching substrate shape.
- Put reaction chamber lid back onto reaction chamber, aligning gas lines and bolt holes
- Loosely put several bolts in lid to ensure alignment, then tighten opposing bolts, to prevent O-ring from binding. Ex: tighten bolt at 6 o'clock, then 12 o'clock, then 9 o'clock and three o'clock, and so on.
- Put new gaskets in VCR connections on all three gas lines entering the reaction chamber.
- Tighten VCR connections finger tight, then, using wrenches, tighten 45°.

HP-MOCVD System Start

- Turn on power switch, located on the wall between the scrubber and gas panels.
- Turn on the chiller (cooling water source).
    - The chiller is located near the XRD machine.
    - Turn the flow valves off.
    - Turn on by pressing on switch.
    - Turn flow valve on.
- Turn on the nitrogen flow to the system.
    - making sure that all line switching valves are directing nitrogen into the HP-MOCVD, not the ZnO reactor.
    - Open the blue hand valve, located on the gas panels, that sends nitrogen to the vacuum pump.
    - The pressure leaving the liquid nitrogen tank should be regulated to 60psi for general purposes, but may read high, until gas starts to flow.
- Turn on Ebara vacuum pump.
    - Close all valves entering or exiting the Ebara vacuum pump: black screw valve underneath the reaction chamber and the blue ball valve in front of the pump.
    - Flip the breaker on the bottom left of the back panel of the pump.
    - If the water (from chiller) and nitrogen are flowing in acceptable amounts, you can press start on the pump's controller. If they are not, an alarm will sound.
        - You can adjust the flow of nitrogen with the black regulator on the back of the pump, but should first ensure that nitrogen is correctly flowing to the pump.

        - If the alarm sounded, press reset, then try to start the pump.
- Turn the MFC's power on.
    - Open the control cabinet and turn on the power strip for the MFCs. All MFCs should start blinking green lights on top if they initialized into the DeviceNET system correctly. This could take several minutes.
- Turn on the Filmetrics in-situ monitoring system.
    - On the Filmetrics system and light sources, ensure that the fiber connected to the front panel is the one that goes to the reaction chamber, which should be labeled "light source InSitu."
    - Make sure that the fiber connected to the back panel of the lower Filmetrics spectrum analyzer is the one receiving light from the reaction chamber, which should be labeled "InSitu XX."
    - Turn on the light source and press the halogen button to turn on the halogen. Open the Shutter.
    - Open the Filmetrics software and select reflection vs. time on the far right pull down menu. Select desired wavelengths for monitoring and press start.
- Open NI Labview HP-MOCVD Control Software.
    - Open the most recent edition of the labview software for controlling the HP-MOCVD.
    - Press start. The green light will light if the entire DeviceNET system initializes, otherwise troubleshooting will be necessary.

Pre-Growth

- Slowly open the black screw valve, underneath the reaction chamber to vacuum out the chamber. Vacuum for at least 10 minutes to ensure significant removal of oxygen.
- Run a fill/purge sequence on the bubbler lines to ensure that all remaining gasses, especially MO are vacuumed out. (fill lines with nitrogen, then vacuum lines out, repeat several times. The process is detailed in after growth section)
- Set susceptor RPMs to desired speed on the microDart motor controller. (we have been using 160-200)
- Start nominal nitrogen flows through chamber.
- Close black screw valve and wait until the chamber pressure reaches desired pressure, or a minimum of 1 atmosphere to prevent any oxygen from backing up into the system.
- Open the blue ball valve.
- Engage heater power supply by pressing the green button on the left side of the front panel.
- Set temperature in labview to ~4 degress above currently measured temperature.
- When temperature starts to move, set deg/sec to 0.5 and set temperature to desired temperature.
- The deg/sec variable can be increased around 100 degrees, usually no more than 0.5 at a time and no farther than 4 deg/sec to avoid melting the heater with sudden, large changes in current.

Growth

- Open the manual bubbler valves for the chemicals that will be used in the growth.
- Plug in the scrubber.
- If a recipe is to be used, load the recipe by selecting load recipe in the mode pull down list in the bottom left of the labview front panel.
- Once the correct recipe is loaded, select run recipe from the same pull down menu.
- If manual growth is desired, the MFC settings and valve opening and closings must be done manually. The total flows through the three lines coming into the reactor must have a ratio of 9-2.5-9, where the MO line and the NH_3 line have 9 units, proportionately.
- Molar gas flows for NH_3 can be determined from simple thermodynamics and from knowing the pressure and temperature of the NH_3. The pressure will be reactor pressure, with the current set-up and the temperature is controlled with a jacket around the NH_3 cylinder that can be read.
- There is a spread sheet that can simply calculate the molar flows through the bubblers, which should be located in the files for the reactor. The temperature of the chemicals is kept constant with a water bath and can be directly read. The pressure is measured with a pressure transducer, and can be read through the NI Labview HP-MOCVD control software.

After Growth

- Set all gas flows to nitrogen.
- Close the manual bubbler valves for the chemicals.
- Set temperature to 0, letting the deg/sec setting be no higher than 4.
- Once the power supply is no longer supplying power to the heater, press the red button on the left side of the front panel to put it in standby mode.
- Run a fill/purge sequence on the bubbler lines, several times to clear any excess MO out of the lines.
    - Make sure the manual bubbler valves are closed.
    - Run the fill and purge sequences ~4 times. Adjust as necessary.
    - Purge Sequence
        - Make sure the manual bubbler valves are closed.
        - Close the pneumatic valves to the reactor.
        - Close the source (N_2) valve.
        - Open the pneumatic valves for the bubbler bypass and to the exhaust.
        - Wait for the MFCs to read no or minimal gas flow (some noise will occur).
    - Fill Sequence
        - Make sure the manual bubbler valves are closed.
        - Close the pneumatic valves to the reactor and to the exhaust.
        - Open the pneumatic bubbler bypass valve.
        - Open the source (N_2) valve and set the MFC to 1slm or higher.
        - Wait for the MFCs to read no or minimal gas flow (some noise will occur).

- Unplug the scrubber.
- Stop the Filmetrics data acquisition by pressing stop. Save any data.
- Press stop on the vacuum pump, but do not stop nitrogen or water flow to the pump, until it cools to 40°C, which can be checked on the pump's controller.
- Do not open reactor until the temperature reading is down to 200°C. This is not the actual temperature at this point, as the thermocouple is not accurate this low. The susceptor will be significantly cooler than this reading.
- Turn off all gas flows in reactor. Press the user stop button in labview, DO NOT PRESS THE STOP SIGN IN THE MENUBAR. LABVIEW RUNS A SEQUENCE TO LOG DEVICES OFF OF DeviceNET THAT DOES NOT RUN IF MENUBAR STOP IS USED. THIS COULD RENDER MFCs UNRESPONSIVE ($2-5k each!)
- Turn off the Filmetrics and light sources, the same way they were turned on.
- Set the microDart's RPMs to 0.
- Open the reaction chamber in the reverse of the way it was closed.
- Remove the sample with wafer tweezers.
- Turn off the power switch.
- Turn off the MFCs. DO NOT DO THIS STEP IF LABVIEW IS STILL ON.
- If the pump has reached 40°C, turn off the pump's breaker, the water chiller in the reverse of its turn on, and the nitrogen.

APPENDIX B: RECIPE FOR InGaN MATERIAL AND MQW GROWTH IN HIGH PRESSURE MOCVD

Table 14: Final InGaN active layer recipes. *Intended to be 870ºC, however 870ºC at 2.5 bar(a) has not yet been grown.

Layer	**Pressure**	**$Temp_{tc}$**	**$Temp_{sub}$**	**V:III***	**MO**	**In:Ga**	**Rpm**
InGaN	1.5 bar-a	930ºC	870ºC	90K	$5\frac{\mu mol}{min}$	1:4	200
InGaN	2.0 bar-a	937ºC	870ºC	120K	$5\frac{\mu mol}{min}$	1:4	200
InGaN	2.5 bar-a	930ºC	839ºC**	150K	$5\frac{\mu mol}{min}$	1:4	200

Table 15: 1.5 bar(a) MQW growth recipe. *V:III ratio note: 12K shows best InGaN structure, determined by XRD (HP77). This was thought to be highly related to roughness. 30K-45K was nominal for many of these experiments. 90K showed greatest PL intensity. **This temperature was intended to be 870ºC, however, since the temperature delta increased with pressure, it was actually grown at 839ºC.

Layer	**Press.**	**$Temp_{tc}$**	**$Temp_{gr}$**	**V:III**	**MO**	**In:Ga**	**Rpm**	**t_{gr}**	
GaN Cap	1.5 bar-a	930ºC	870ºC	90K*	$5\frac{\mu mol}{min}$	1:4	200	860s	
InGaN Active	1.5 bar-a	930ºC	870ºC	90K*	$5\frac{\mu mol}{min}$	1:4	200	260s	x4
GaN Barrier	1.5 bar-a	930ºC	870ºC	90K*	$5\frac{\mu mol}{min}$	1:4	200	860s	
GaN ↓Temp	1.5 bar-a	1100ºC -930ºC	1066ºC -870ºC	30K	$8\frac{\mu mol}{min}$	0:1	200	3-6 min	
HT GaN	1.5 bar-a	1100ºC	1066ºC	30K	$8\frac{\mu mol}{min}$	0:1	200	20 min	
MOCVD/HVPE GaN on Al_2O_3 Template									

APPENDIX C: SAMPLE GROWTH PARAMETERS AND STRUCTURES

Table 16: Growth structures and parameters for samples included in this research

Samp	Structure	Press Bar(a)	V:III	In:Ga	III-Flux	T_{tc} ºC	T_{est} ºC	rpm
HP11	InGaN 11m 25s on GaN template	1.5	7.56k	3:1	59.8	750	630	200
HP13	InGaN 11m 25s on GaN template	1.5	7.56k	3:1	59.8	870	750	200
HP17	InGaN 6m 25s on GaN template	1.5	30.25k	3:1	15	870	750	200
HP23	GaN buffer, InGaN, GaN cap, 20nm each	1.5	30.25k	3:5	15	900	780	200
HP38	InGaN on GaN template	1.5	45.10k	1:5	10	775	700	160
HP39	InGaN on GaN template	1.5	45.10k	1:5	10	900	775	160
HP40	InGaN on GaN template	1.5	45.10k	1:5	10	930	800	160
HP52	4QWs on HT GaN buffer. Capped with GaN. 10m Active (A), 3m Barrier &Cap (B), 16m30s HT GaN (C)	1.5	A: 45k B: 38k C: 30k	1:2	A:12 B:10 C:10	A, B: 930 C: 1100	A, B: 800 C: 980	160

HP53	4QWs on HT GaN buffer. Capped with GaN. 10m Active (A), 3m Barrier &Cap (B), 16m30s HT GaN (C)	1.5	A: 45k B: 38k C: 30k	1:2	A:12 B:10 C:10	A, B: 930 C: 1100	A, B: 800 C: 980	160
HP54	4QWs, capped with GaN. 10nm Active, 3nm Barrier &Cap	1.5	45.10k	1:4	10	930	800	160
HP55	4QWs, capped with GaN. 10nm Active, 3nm Barrier &Cap	1.5	45.10k	1:4	10	950	820	160
HP56	4QWs on LT GaN buffer. Capped with GaN. 5m Active, 1m30s Barrier &Cap, 5m LT GaN	1.5	45.10k	1:4	10	930	800	160
HP57	4QWs on HT GaN buffer. Capped with GaN. 5m Active (A), 1m30s Barrier &Cap (B), 5m HT GaN (C)	1.5	A: 45k B, C: 30k	1:4	A,B: 10 C:15	A,B: 930 C: 1100	A,B: 800 C: 980	160

HP61	Buffer Layer DOE 5m Cap (A) [1m30s Active (B) 5m Barrier (C)] x4 2m Buffer (D)	1.5	A,C,D: 30k B: 45k	1:4	A,B, C: 10 D: 15	A,B,C: 930 D: 1200	x	160
HP62	Buffer Layer DOE 5m Cap (A) [1m30s Active (B) 5m Barrier (C)] x4 10m Buffer (D)	1.5	A,C,D: 30k B: 45k	1:4	A,B, C: 10 D: 15	A,B,C: 930 D: 1200	x	160
HP63	Buffer Layer DOE 5m Cap (A) [1m30s Active (B) 5m Barrier (C)] x4 10m Buffer (D)	1.5	A,C,D: 30k B: 45k	1:4	A,B, C: 10 D: 15	A,B,C: 930 D: 1100	x	160
HP64	Buffer Layer DOE 5m Cap (A) [1m30s Active (B) 5m Barrier (C)] x4 2m Buffer (D)	1.5	A,C,D: 30k B: 45k	1:4	A,B, C: 10 D: 15	A,B,C: 930 D: 1100	x	160
HP76	14m 20s Cap (A) [4m20s Active (B) 14m 20s Barrier (C)] x4 -1C/s Transition (D) 20m Buffer (E)	1.5	A,B,C: 90k D, E: 30k	1:4	A,B, C: 5 D,E: 8	A,B,C: 930 D: 1100-930 E: 1100	x	200

HP78	14m 20s Cap (A) [4m20s Active (B) 14m20s Barrier (C)] x4 -1C/s Transition (D) 20m Buffer (E)	2.0	A,B,C: 150k D, E: 125k	1:4	A,B, C: 5 D,E: 6	A,B,C: 930 D: 1100-930 E: 1100	x	200
HP79	14m 20s Cap (A) [4m20s Active (B) 14m 20s Barrier (C)] x4 -1C/s Transition (D) 20m Buffer (E)	2.5	A,B,C: 120k D, E: 100k	1:4	A,B, C: 5 D,E: 6	A,B,C: 930 D: 1100-930 E: 1100	x	200